The ALOG family members OsG1L1 and OsG1L2 regulate inflorescence branching in rice

Veronica Beretta, Emanuela Franchini, Israr Ud Din, Elia Lacchini, Lisa van den Broeck, Rosangela Sozzani, Gregorio Orozco-Arroyo, Elisabetta Caporali, Hélène Adam, Stefan Jouannic, et al.

the plant journal

SEB SOCIETY FOR EXPERIMENTAL BIOLOGY

The Plant Journal (2023) doi: 10.1111/tpj.16229

The ALOG family members *OsG1L1* and *OsG1L2* regulate inflorescence branching in rice

Veronica M. Beretta[1,†], Emanuela Franchini[1,†], Israr Ud Din[1,†,‡], Elia Lacchini[1,¶], Lisa Van den Broeck[2], Rosangela Sozzani[2], Gregorio Orozco-Arroyo[1], Elisabetta Caporali[1], Hélène Adam[3], Stefan Jouannic[3], Veronica Gregis[1] and Martin M. Kater[1,*]

[1]*Dipartimento di Bioscienze, Università degli Studi di Milano, Via Celoria 26, 20133 Milano Italy,*
[2]*Plant and Microbial Biology Department, North Carolina State University, Raleigh NC 27695 USA, and*
[3]*DIADE, University of Montpellier, IRD, CIRAD, Montpellier France*

Received 23 September 2022; revised 21 March 2023; accepted 24 March 2023.
*For correspondence (e-mail martin.kater@unimi.it).
†These authors contributed equally to this work.
‡Present address: Institute of Biotechnology and Genetic Engineering (IBGE), University of Agriculture, Peshawar 25130 Pakistan
¶Present address: VIB Center for Plant Systems Biology, Technologiepark 71, B-9052 Ghent Belgium

SUMMARY

The architecture of the rice inflorescence is an important determinant of crop yield. The length of the inflorescence and the number of branches are among the key factors determining the number of spikelets, and thus grains, that a plant will develop. In particular, the timing of the identity transition from indeterminate branch meristem to determinate spikelet meristem governs the complexity of the inflorescence. In this context, the *ALOG* gene *TAWAWA1* (*TAW1*) has been shown to delay the transition to determinate spikelet development in *Oryza sativa* (rice). Recently, by combining precise laser microdissection of inflorescence meristems with RNA-seq, we observed that two *ALOG* genes, *OsG1-like 1* (*OsG1L1*) and *OsG1L2*, have expression profiles similar to that of *TAW1*. Here, we report that *osg1l1* and *osg1l2* loss-of-function CRISPR mutants have similar phenotypes to the phenotype of the previously published *taw1* mutant, suggesting that these genes might act on related pathways during inflorescence development. Transcriptome analysis of the *osg1l2* mutant suggested interactions of *OsG1L2* with other known inflorescence architecture regulators and the data sets were used for the construction of a gene regulatory network (GRN), proposing interactions among genes potentially involved in controlling inflorescence development in rice. In this GRN, we selected the homeodomain-leucine zipper transcription factor encoding the gene *OsHOX14* for further characterization. The spatiotemporal expression profiling and phenotypical analysis of CRISPR loss-of-function mutants of *OsHOX14* suggests that the proposed GRN indeed serves as a valuable resource for the identification of new proteins involved in rice inflorescence development.

Keywords: *Oryza sativa*, transcription factor, inflorescence architecture, meristem identity, transcriptome analysis, CRISPR mutants, gene regulatory network, *ALOG*.

INTRODUCTION

The inflorescences of land plants show a wealth of distinct architectures, evidencing their importance for reproductive success. The plant species- or family-specific inflorescence shape depends on the identity and activity of the meristems, which determine the degree of branching and the number of flowers that will ultimately develop. Inflorescence meristems (IMs) are defined as indeterminate, as they continue to develop meristems in the axils of lateral organs, such as bracts. In contrast, floral meristems (FMs) are determinate, as the development of the floral organs exhausts the meristematic activity. In this sense, the formation of flowers can be seen as a developmental end point. An extreme example is that of tulips, where the apical meristem transforms into an FM and forms one single apical flower. It is thus the transition from indeterminate to determinate meristems that defines the complexity of an inflorescence (Hake, 2008).

Oryza sativa, commonly known as rice, develops a complex and determinate inflorescence, named panicle (Bommert et al., 2005; Han et al., 2014). Its architecture is established during early stages of rice reproductive development, and it depends on the activity of different meristem types (Caselli et al., 2020; Tanaka et al., 2013). During

the floral transition, the rice shoot apical meristem (SAM) becomes an IM, also called a rachis meristem. The IM gives rise to primary branch meristems (PBMs) that produce axillary meristems (AMs), which could differentiate into indeterminate secondary branch meristems (SBMs) or determinate spikelet meristems (SMs). In the same way, SBMs elongate and produce SMs. In rice, the SM develops three FMs, one of which will differentiate into one fertile floret, whereas the other two will develop into empty glumes (sterile lemmas), thus exhausting the pool of meristematic cells (Bommert et al., 2005; Han et al., 2014). Furthermore, the length of the rice inflorescence, and consequently the number of PBs that can develop, is also determined by the timing of IM abortion, with the formation of an undifferentiated dome.

Rice plants in which an early transition to SM identity occurs will develop panicles that are less complex, with fewer grains, in contrast to plants in which the transition is delayed. Among the genes that have been identified to control this transition are *ABERRANT PANICLE ORGANIZATION 1* (*APO1*) and *APO2* (Ikeda-Kawakatsu et al., 2012). Both are mainly expressed in IMs and in BMs, where they also promote cellular proliferation. They are orthologs of the *Arabidopsis thaliana* genes *UNUSUAL FLORAL ORGANS* (*UFO*) and *LEAFY* (*LFY*), respectively. However, whereas *UFO* and *LFY* promote floral identity, *APO1* and *APO2* repress the transition to determinate SM formation (Ikeda-Kawakatsu et al., 2009, 2012). Recently, it was shown that LARGE2, a HECT-domain E3 ubiquitin ligase OsUPL2, interacts directly with APO1 and APO2 to modulate their stability. Genetic analysis of the *large2* mutant, which displays bigger panicles with more branches and grains, confirmed that *LARGE2* functions in a common pathway with *APO1* and *APO2* (Huang et al., 2021). *TAWAWA 1* (*TAW1*)/*G1-LIKE 5* (*G1L5*) is another gene that promotes BM identity and suppresses SM specification by activating genes involved in the repression of floral transition (Yoshida et al., 2013). The dominant *taw1-D* gain-of-function mutant shows a delay in spikelet specification, which results in increased branching and higher grain numbers. *TAW1* belongs to the *Arabidopsis LSH1 and Oryza G1* (*ALOG*) gene family, which includes 14 *ALOG* genes in rice. The ALOG domain is highly conserved among land plants and evolutionary studies propose that it is derived from the N-terminal DNA-binding domain of integrases that belong to the tyrosine recombinase superfamily, which are encoded by a distinct type of DIRS1-like LTR retrotransposon found in several eukaryotes (Iyer & Aravind, 2012; Naramoto et al., 2020).

Harrop et al. (2016) used laser microdissection microscopy to specifically isolate different rice IM tissues for expression profiling with RNA-seq. Subsequent transcriptome analysis revealed that two *ALOG* genes, *OsG1L1* and *OsG1L2*, have similar expression profiles as *TAW1*. All three genes are highly expressed in the IM and, subsequently, their expression gradually decreases in the PBMs, the elongated PBMs with AMs (ePBMs/AMs) and the SMs. Phylogenetic analysis showed that *OsG1L1* and *OsG1L2* both cluster in subgroup A and are therefore more distantly related to *TAW1*, which belongs to subgroup C (Li et al., 2019).

Here, we describe the functional analysis of *OsG1L1* and *OsG1L2*, which provides evidence that both genes play a similar role in rice inflorescence development. As in the *taw1-3* and *TAW1* RNAi lines, both *osg1l1* and *osg1l2* CRISPR-Cas9 mutants showed a reduced branching phenotype and lower grain numbers. RNA-seq analysis of developing *g1l2* inflorescences was used to model a gene regulatory network (GRN). Validation of the resulting network by the functional characterization of the homeodomain-leucine zipper transcription factor (TF) gene *OsHOX14* suggests that the proposed GRN could serve as a valid resource for the identification of genes controlling inflorescence development in rice.

RESULTS

OsG1L1 and *OsG1L2* expression analysis

Previous transcriptome analysis of laser microdissected rice reproductive meristems allowed the identification of two *ALOG* genes, *OsG1L1* and *OsG1L2*, that share a similar expression profile with the previously studied *TAW1* gene (Harrop et al., 2016; Yoshida et al., 2013; Figure 1a). These genes are highly expressed in the IM, then mRNA abundance decreases in the PBM and a further reduction is observed in the ePBMs/AMs. In the SM there is a slight increase in mRNA levels for all three genes.

To determine the expression profile of *OsG1L1* and *OsG1L2* in more detail and to confirm their expression in reproductive meristems, we performed real-time PCR on different plant tissues, such as the root, the root tip (where the root apical meristem is localized), young and mature leaves, the SAM, and all reproductive meristem-enriched tissues, like IM, PBM, ePBM/AM, SM/FM, and milk and mature grains, respectively, at 8 and 30 days after fertilization. The different meristem- enriched tissues were collected following the time points defined for the Nipponbare cultivar, as described previously (Harrop et al., 2016), and the correct developmental stage was checked using a stereomicroscope. As the expression of *TAW1* was already described (Yoshida et al., 2013), it was used as a positive control. This analysis showed that all three genes are preferentially expressed in IM tissues (Figure 1b).

RNA *in situ* hybridization was performed to further investigate and compare the spatiotemporal expression of *OsG1L1*, *OsG1L2* and *TAW1* during different stages of panicle development. We designed for each of the three genes

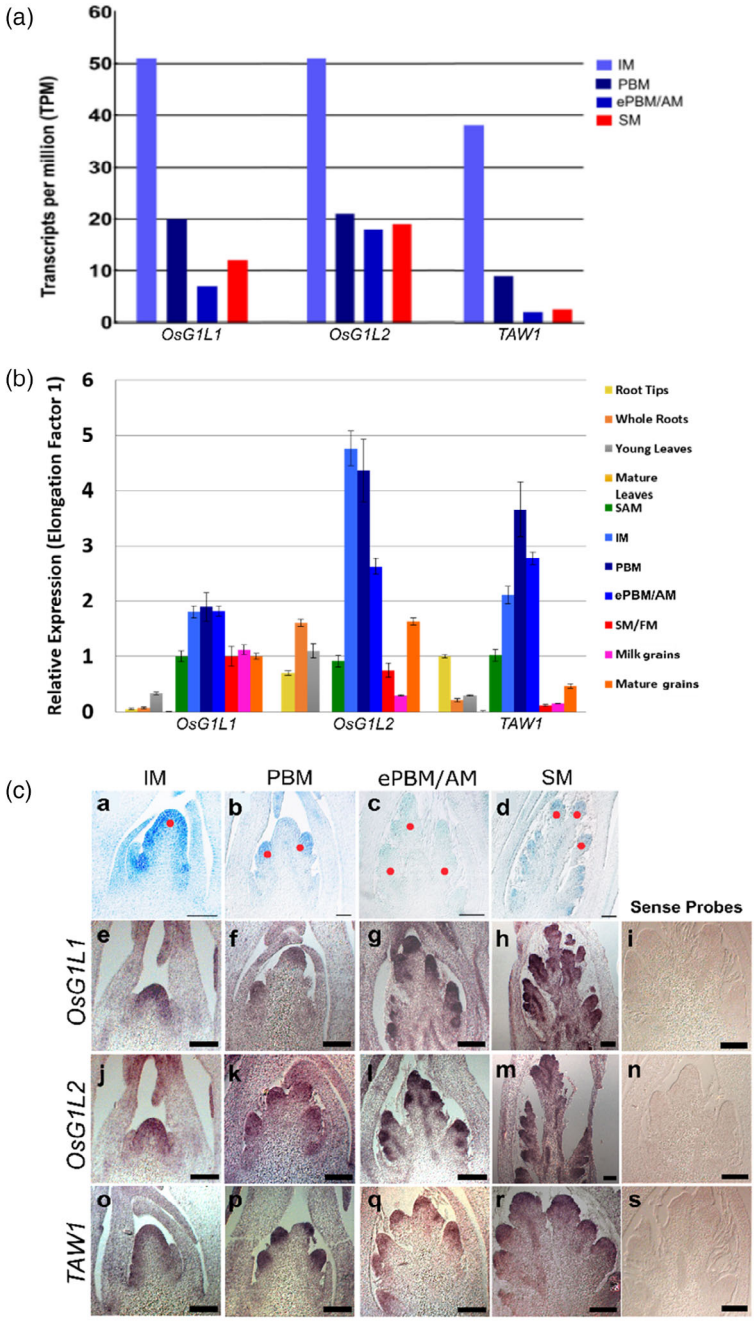

Figure 1. The genes *OsG1L1*, *OsG1L2* and *TAW1* of the *ALOG* family are highly expressed in reproductive meristems.
(a) *OsG1L1* and *OsG1L2* expression in four reproductive meristem types, analyzed by RNA-seq (Harrop et al., 2016). Read counts are presented in transcripts per million.
(b) *OsG1L1*, *OsG1L2* and *TAW1* expression measured by RT-qPCR in different tissues: vegetative tissues (roots and leaves), manually dissected inflorescence meristem (IM), primary branch meristem (PBM), elongated PBM with axillary meristem (ePBM/AM), spikelet meristem/floral meristem (SM/FM) and grains.
(c) Expression pattern of *OsG1L1*, *OsG1L2* and *TAW1* analyzed by *in situ* hybridization in the four developmental stages that are presented in (a) and described in the text. Red dots indicate different meristematic tissues: a, IM; b, PBM; c, ePBM/AM; and d, SM. e–h, *OsG1L1* antisense probe; l, *OsG1L1* sense negative control probe; j–m, *OsG1L2* antisense probe; n, *OsG1L2* sense negative control probe; o–r, *TAW1* antisense positive control probe; s, *TAW1* sense negative control probe. Scale bars: a–c, 50 μm; d–s, 100 μm.

a specific digoxigenin-labeled RNA probe. This analysis revealed that *OsG1L1* and *OsG1L2* have similar expression profiles to that of *TAW1*. All three genes are expressed in the IM, PBM, ePBM/AM and SM/FM, suggesting that *OsG1L1* and *OsG1L2* might have a similar functional role in the reproductive meristems as *TAW1* (Figure 1c).

Analysis of the *osg1l1* and *osg1l2* mutant phenotypes

To functionally characterize *OsG1L1* and *OsG1L2*, CRISPR-Cas9 genome editing technology was used to generate mutations in these genes. A specific single-guide RNA (sgRNA) was designed for each gene and the two CRISPR constructs (Miao et al., 2013) were used for *Agrobacterium tumefaciens*-mediated transformation of rice embryonic calli. The two sgRNAs were designed to create indels in the ALOG domain.

The sgRNA designed for *OsG1L1* targeted the first exon at 397 bp from the ATG start site, whereas the sgRNA for *OsG1L2* was designed to target a region 131 bp downstream from the ATG start site (Figures S1 and S2). For *OsG1L1*, five T_0 transgenic plants with different mutations at the sgRNA target site were obtained. Three of these plants present in-frame mutations (3- and 6-bp deletions) and were not further analyzed. Two independent transformants had a homozygous deletion of 2 bp (AG) at 145 bp from the translation start site. This mutation created a frameshift resulting in the formation of an aberrant protein, characterized by the disruption of the ALOG domain and of the putative nuclear localization signal (NLS). For these reasons, the aberrant protein obtained is most likely not functional (Figure S1). For further analysis we used the two *osg1l1* mutants that present an AG homozygous deletion and in the T_2 generation we obtained homozygous plants without the Cas9-encoding T-DNA insertion.

For the CRISPR construct targeting *OsG1L2*, 18 T_0 transgenic rice plants were generated. All these plants had a similar frameshift mutation through the insertion of a single base pair (A, C, G or T) at 148 bp from the start site. The insertion of A leads to the formation of a premature stop codon (TGA), resulting in the production of a truncated protein of 49 amino acids (Figure S2) lacking the ALOG domain and the putative NLS. The insertion of one of the other bases (C, G or T) leads to the formation of a protein of 176 amino acids without the ALOG domain and the putative NLS (Figure S2). In the T_1 generation we selected two independent *osg1l2* mutant lines having an A or C insertion. In the T_2 generation we obtained lines homozygous for these insertions and without the Cas9-encoding T-DNA insertion. For detailed phenotyping we used the line with the insertion of A.

Considering that the expression of *OsG1L1* and *OsG1L2* was predominant in the reproductive meristem tissues, a detailed phenotypic analysis of the panicle was performed using P-TRAP (Figure 2; A L-Tam et al., 2013). To obtain a robust statistical analysis, at least 15 plants for each genotype were analyzed. In particular, we analyzed 15 wild-type plants, 19 *osg1l1* mutants and 20 *osg1l2* mutants. After panicle imaging, P-TRAP was used to quantify the traits related to panicle architecture and grain numbers (Table S1).

This analysis showed that *osg1l1* and *osg1l2* produced significantly shorter panicles than wild-type plants. Furthermore, their panicles developed fewer PBs, SBs and spikelets. In particular, the *osg1l1* mutants produced panicles that were on average 2 cm shorter than the wild type and developed on average three PBs and 30 spikelets fewer than wild-type plants. Interestingly, the number of SBs did not significantly differ from that of the wild type (Figure 2c–f).

The *osg1l2* mutant plants produced panicles that were on average 1.5 cm shorter than the wild type and developed on average four PBs, eight SBs and 51 spikelets fewer than wild-type plants (Figure 2c–f). This analysis confirmed a previous independent experiment in which PBs, SBs and spikelets numbers were compared between wild-type and *osg1l2* plants with a different mutation (C inserted 148 bp from the ATG) (Figure S3).

The P-TRAP analysis also revealed that both *osg1l1* and *osg1l2* mutant lines had longer PBs and SBs as well as longer internodes in PBs (Figure 2g–i). In detail, the *osg1l1* mutant plants displayed PBs and SBs that were, on average, 1.0 and 0.5 cm longer, respectively, than those of wild-type rice plants. The internodes of PBs were on average 0.4 cm longer than in the wild type. The *osg1l2* mutant plants instead produced PBs and SBs that were, on average, 1.6 and 1.0 cm longer than in the wild type, respectively. The internodes of PBs were on average 0.7 cm longer than in the wild type. Overall, both mutants showed similar aberrations in panicle architecture, although the phenotype of the *osg1l2* mutant was more severe.

We also investigated whether the loss of function of OsG1L1 and OsG1L2 affects grain size. We compared the length, width and surface area of *osg1l1* and *osg1l2* grains with those of the wild type. This analysis revealed that *osg1l1* and *osg1l2* mutants produced significantly smaller grains than the wild type. Both *osg1l1* and *osg1l2* grains had smaller areas, where *osg1l1* grains had a reduced length and width and *osg1l2* grains only showed a reduction in grain width, compared with the wild type (Figure S4).

As *OsG1L1* and *OsG1L2* were preferentially expressed in the IMs, we decided to focus our attention on the development of the panicle.

Comparative analysis of *OsG1L1*, *OsG1L2* and *TAW1* function in reproductive meristems

It has been shown that *TAW1*, which shares a similar expression profile with *OsG1L1* and *OsG1L2*, is a suppressor of the phase change from branch meristems to SM identity (Yoshida et al., 2013). As the panicle architecture phenotype of the *osg1l1* and *osg1l2* mutants was similar to the *taw1-3* mutant, we investigated the possibility that these three *ALOG* genes act in the same pathway.

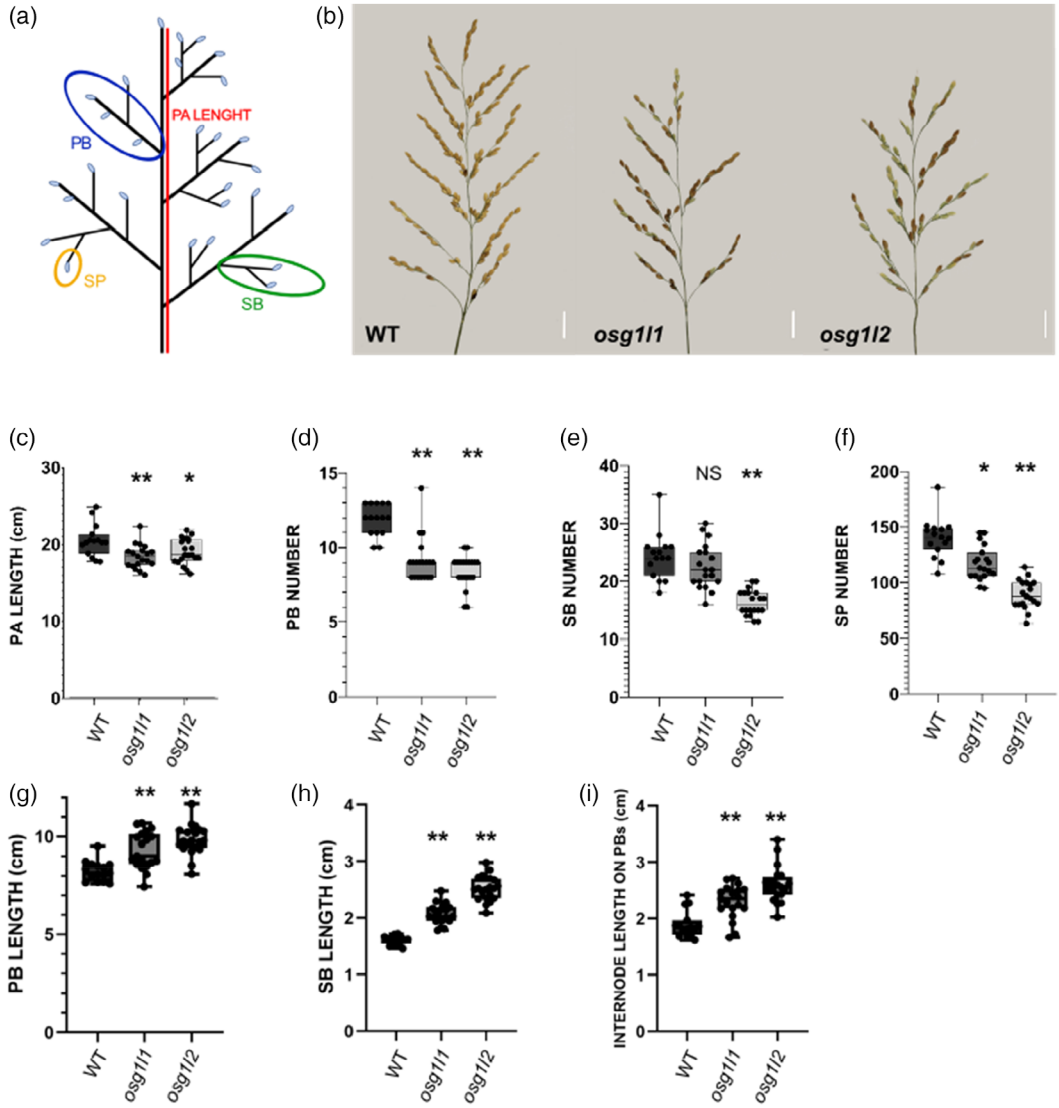

Figure 2. Phenotypical analysis of panicle architecture in the wild type (WT) and in the *osg1l1* and *osg1l2* mutants.
(a) Schematic representation of panicle structure. PA, panicle; PB, primary branches; SB, secondary branches; SP, spikelets.
(b) Main panicles of WT, *osg1l1* and *osg1l2* (2 cm scale bars). Graphs represent comparisons of: (c) panicle (PA) length; (d) primary branch (PB) number; (e) secondary branch (SB) number; and (f) spikelet (SP) number in WT, *osg1l1* and *osg1l2* backgrounds. Graphical representation of the comparison between: (g) length of PB; (h) length of SB; and (I) length of the internodes in PBs. One-way analysis of variance (ANOVA) with Tukey's test: $^{**}P < 0.01$; $^{*}P < 0.05$.

In the dominant overexpression mutant *taw1-D1*, three *SHORT VEGETATIVE PHASE* (*SVP*) genes, *OsMADS22*, *OsMADS47* and *OsMADS55*, were upregulated (Yoshida et al., 2013). To investigate whether these genes are deregulated in the *osg1l1* and *osg1l2* mutants, we performed a real time quantitative PCR (RT-qPCR) analysis using three biological replicates of developing inflorescences enriched in PBMs and ePBMs/AMs of wild-type, *osg1l1* and *osg1l2* plants. There were no significant differences in the expression of the three *SVP* genes in the *osg1l1* and *osg1l2* backgrounds, compared with the wild type. Only *OsMADS22* seems to present a trend of upregulation, just in the *osg1l1* background, but this was not statistically significant (Figure S5).

Yoshida et al. (2013) showed that in *taw1-D1*, *TAW1* overexpression led to a delay in the phase change from BMs to SMs. To determine whether *OsG1L1* and *OsG1L2* are also involved in this phase transition, we performed an *in situ* hybridization using developing panicles at the ePBMs/AMs stage in wild-type, *osg1l1* and *osg1l2* backgrounds using a digoxigenin-labeled RNA probe specific for *FRIZZY PANICLE* (*FZP*). *FZP* encodes for a protein containing an *APETALA 2/ETHYLENE RESPONSE FACTOR* (*AP2/ERF*) domain and has a precise expression pattern that

marks the specification of the SM (Bai et al., 2016; Fujishiro et al., 2018; Komatsu et al., 2003). The developing panicles were harvested 16 days after floral induction. In the *osg1l1* and *osg1l2* backgrounds, we observed an increase in *FZP* expression spots that mark the specification of SMs at the ePBM/AM stage. This suggests that the overall developmental program that leads to the switch from indeterminate to determinate meristems occurs earlier in the two mutants than in the wild type (Figures 3a–c and S6). The earlier specification of the SMs in the *osg1l1* and *osg1l2* mutants was further evidenced by scanning electron microscopy (SEM) (Figure 3d–i). A whole developing panicle was harvested and scanned from each plant (Figure 3d–f). Altogether, our analyses clearly demonstrated that both *OsG1L1* and *OsG1L2* are involved in maintaining the indeterminate state of reproductive meristems.

Transcriptome analysis of the *osg1l2* mutant at early stages of inflorescence development

The phenotypic analysis of the *osg1l1* and *osg1l2* mutants suggests that both genes may play a similar role during rice inflorescence development. As inflorescence branching was more severely affected in the *osg1l2* mutant, this line was selected for RNA-seq transcriptome analysis to obtain deeper insights into the role that this *ALOG* gene plays at the early stages of panicle development.

Developing inflorescences enriched in PBMs and ePBMs/AMs of the wild type and the *osg1l2* mutant were manually dissected. Four biological replicates were collected, each replicate consisting of between eight and 10 dissected inflorescences. Subsequently, RNA was extracted and used for Illumina sequencing (https://www.illumina.com).

The raw RNA-seq files were processed using the TuxNet interface (Spurney et al., 2019). Reads were cleaned, mapped on the *O. sativa* reference genome (IRGSP-1.0), normalized and then fragment per kilobase of transcript per million mapped reads (FPKMs) were calculated (Table S3). Finally, performing a pairwise differential expression analysis between the wild type and the mutant, the TuxNet interface generated data sets of differentially expressed genes (DEGs) (Spurney et al., 2019) (Table S4).

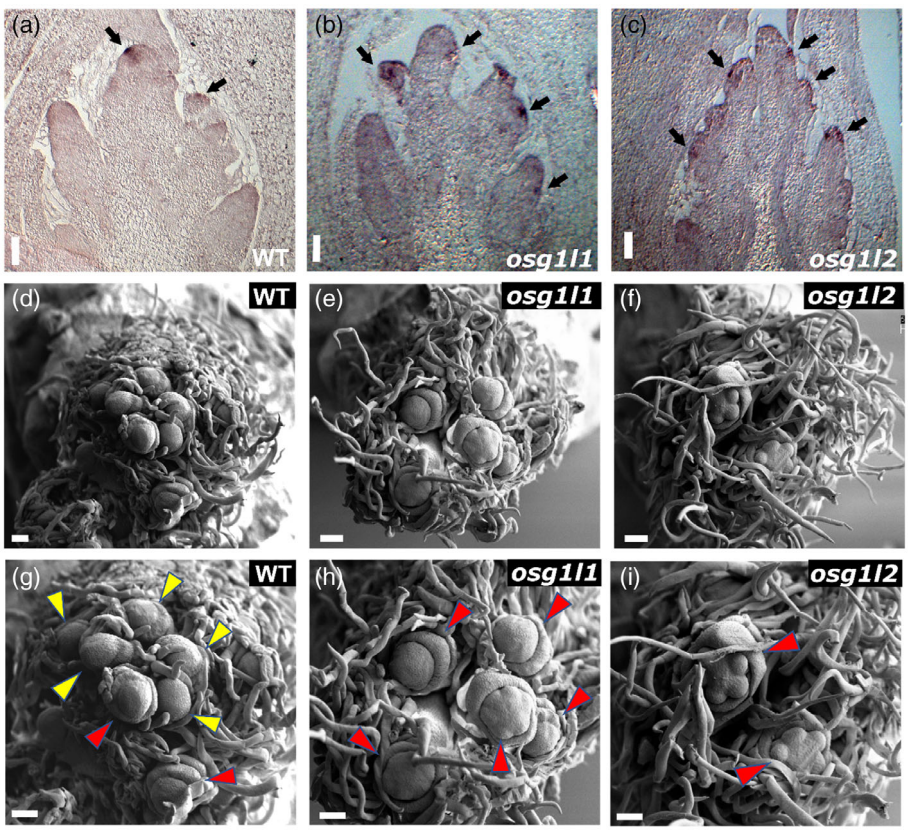

Figure 3. Expression pattern of *FZP* analyzed by *in situ* hybridization at the elongated primary branch meristem with axillary meristem (ePBM/AM) stage in: (a) wild type (WT); (b) *osg1l1* (b); and (c) *osg1l2*. Scale bars: 50 μm. Black arrows indicate *FZP* signal.
Scanning electron microscopy analysis of rice reproductive meristems, collected 16 days after flowering induction under short-day conditions in WT (d, g), *osg1l1* (e, h) and *osg1l2* (f, i) backgrounds (g, h and i show an enlargement of the meristems presented in d, e and f, respectively). Yellow arrows indicate meristems at the indeterminate stage. Red arrows indicate meristems that have already reached the determinate stage. In (e) and (f), stamen primordia are visible. Scale bars: 50 μm.

Table 1 Differentially expressed genes in the *osg1l2* mutant that are involved in inflorescence development

Gene name	Gene ID	$\log_2$(fold change)	*q*-value*	Putative function
OsESP	Os01g0356951	6.55E + 04	0.00245724	Involved in the regulation of panicle architecture
OsMADS37	Os08g0531900	1.87E + 00	0.00245724	Homolog of *FLC* in rice
OsG1L4	Os04g0516200	1.34E + 00	0.00245724	Protein of unknown function, DUF640 domain-containing protein
OsERF112	Os12g0603300	1.09E + 00	0.00245724	Similar to AP2 domain-containing protein
OSRR3	Os02g0830200	1.95E + 00	0.00245724	A-type response regulator involved in cytokinin signaling
OsNAC120	Os10g0477600	−2.47E + 00	0.00245724	Similar to NAM/CUC2-like protein
OsTB1	Os03g0706500	−1.12E + 00	0.00245724	*TCP* family transcription factor, negative regulator of lateral branching
OsMADS34/PAP2	Os03g0753100	−1.13E + 00	0.00245724	MADS-box transcription factor, involved in inflorescence and spikelet development
OsRCN1	Os11g0152500	−1.04E + 00	0.00245724	Putative phosphatidylethanolamine-binding protein, rice *TFL1/CEN* homolog. Involved in inflorescence architecture development and in the repression of flowering
OsRCN4	Os04g0411400	−1.48E + 00	0.00839011	Terminal flower 1-like protein
OsHOX14	Os07g0581700	−1.53E + 00	0.00456853	Homeodomain-leucine zipper (HD-Zip) transcription factor, may be involved in the regulation of panicle development
OsGATA7	Os10g0557600	−1.49E + 00	0.00245724	*GATA* transcription factor. Involved in brassinosteroid-mediated growth regulation, panicle development and grain shape/number/weight/yield
OsIAA14	Os03g0797800	−1.44E + 00	0.00245724	Protein belonging to the AUX/IAA protein family

*A significance cut-off value of 0.05 is applied.

After data processing, on average approximately 13 000 000 reads for each replicate were obtained. The alignment of the reads with the reference genome resulted in >97% coverage overall. Setting the $\log_2$ (fold change, FC) equal to 1 and the *q*-value equal to 0.05, a total of 246 DEGs were identified, 128 of which were downregulated and 118 of which were upregulated in the *osg1l2* mutant, compared with the wild type. Among the upregulated genes in the *osg1l2* mutant, we identified *OsMADS37*, a MADS-box TF encoding a gene homologous to Arabidopsis *FLOWERING LOCUS C* (*FLC*; Ruelens et al., 2013), and *OsG1L4*, another member of the *ALOG* gene family. Interestingly, *EPIGENETIC SHORT PANICLE* (*OsESP*), a putative long non-coding RNA, the overexpression of which leads to shorter and denser panicles, was also upregulated in the *osg1l2* mutant (Luan et al., 2019). Moreover, the expression of genes involved in hormonal pathways was upregulated, such as *OsRR3*, an A-type response regulator that acts as a negative regulator of cytokinin signaling (Cheng et al., 2010). Among the upregulated genes are several genes that encode for zinc-finger transporter proteins and genes encoding for proteins containing an NB-ARC domain, which is associated with plant disease resistance (Van Ooijen et al., 2008) (Table S4; Table 1).

Among the downregulated genes, we found genes encoding TFs like OsNAC120 that are similar to the NAM/CUC-2 like proteins, which have been shown to control plant growth and development in response to biotic and abiotic stresses (Ooka et al., 2003), and a member of the TCP family, *OsTB1/FC1* (that henceforth will be referred to as *OsFC1*). Interestingly, *OsFC1* is already known to be a negative regulator of tillering and inflorescence development (Cui et al., 2020; Takeda et al., 2003). Notably, the TFs *OsMADS34/PAP2* and *OsGATA7*, which are known to be involved in the establishment of inflorescence architecture, and *OsHOX14*, which has been proposed to be involved in panicle development, were also downregulated (Gao et al., 2010; Kobayashi et al., 2012; Shao et al., 2018; Zhang et al., 2018; Zhu et al., 2022). Additional downregulated genes that have been associated with inflorescence development are *OsRCN1* and *OsRCN4* (putative phosphatidylethanolamine-binding protein and rice TFL1/CEN homolog) (Nakagawa et al., 2002). Moreover, genes involved in hormonal pathways like *OsIAA14*, belonging to the Aux/IAA family, and involved in the auxin response, were deregulated (Jain et al., 2006) (Table S4; Table 1).

GRN inference predicts a functional role for *OsHOX14*

To identify major regulatory TFs underlying the inflorescence phenotype of *osg1l2*, we built a GRN using a regression tree with the random forest approach (Spurney et al., 2019). Specifically, we inferred causal relationships between 15 identified differentially expressed TFs, with $\log_2(FC) > 1$ or <-1 and $q < 0.05$, and 232 downstream genes in the *osg1l2* mutant, with $\log_2(FC) > 1$ or <-1 and $q < 0.05$. The inferred network contained 79 genes, of which five TFs have more than 10 outgoing regulations, including *OsWRKY80* (Wu et al., 2005), *OsG1L2*, *OsMADS37* (Ruelens et al., 2013), *OsFC1* (Cui et al., 2020; Takeda et al., 2003) and *OsGATA7* (Zhang et al., 2018) (Figure 4). One of these major regulators is *OsG1L2*, regulating 16 downstream genes, several of which have been shown to be involved in rice inflorescence development (Figure 4c). For example, *OsESP* is a putative long non-coding RNA, the gain-of-function mutant

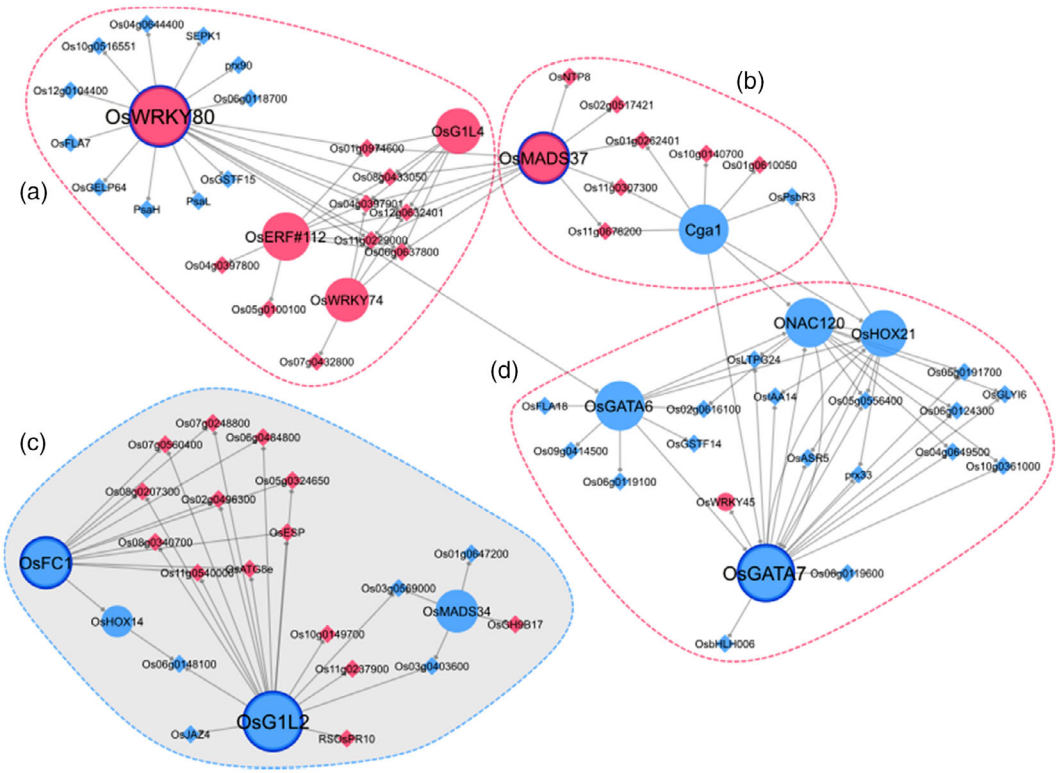

Figure 4. Graphic representation of the predicted gene regulatory network (GRN).
Regulatory interactions were inferred using a regression tree with random forest approach. Transcription factors and other genes are represented by circles and diamonds, respectively. The interactions are represented by a diamond arrow. Upregulated and downregulated genes are highlighted in magenta and blue, respectively. Encircled with dotted lines are the four major subclusters (a–d) into which the network can be divided. Circled in dark blue, with a continuous line, are the five major transcription factors of the GRN: *OsWRKY80*, *OsG1L2*, *OsMADS37*, *OsFC1* and *OsGATA7*. The module containing *OsG1L2* is highlighted in gray (c).

of which leads to a short and denser panicle (Luan et al., 2019), and *OsJAZ4*, also known as *OsTIFY11b*, is a positive regulator of grain size, acting downstream of *TRIANGULAR HULL 1* (*OsTH1*), another ALOG factor (Hakata et al., 2012; Wang et al., 2019). Interestingly, 13 of the predicted OsG1L2 targets are upregulated in the *osg1l2* mutant, 10 of which are predicted to be co-regulated by *OsFC1*, a gene known to negatively regulate branching (Cui et al., 2020; Takeda et al., 2003).

To identify regulatory subclusters within the *osg1l2* network, we clustered the network genes into different modules with the CYTOSCAPE plug-in CLUSTERMAKER 2 (see Experimental procedures) (Figure 4). A total of four modules were identified: one smaller module of 10 genes (Figure 4b) and three larger modules of 24, 23 and 22 genes (Figure 4a, c,d). The smaller module contains *CYTOKININ-RESPONSIVE GATA TRANSCRIPTION FACTOR 1* (*OsCGA1*), the constitutive overexpression of which reduced grain filling (Hudson et al., 2013), and *OsMADS37*, the closest homolog of Arabidopsis *FLC* (Shrestha et al., 2014) (Figure 4b). One of the largest modules contains two *GATA* TFs, *OsGATA6* and *OsGATA7*, which were recently reported to influence plant architecture and grain shape by regulating cell proliferation, and of which CRISPR/Cas9 lines show a similar phenotype to that of *osg1l2* (Zhang et al., 2018; Zhang et al., 2022) (Figure 4d). As we were interested in the regulatory interactions underlying the *osg1l2* mutant phenotype, we focused on module C, which contains four TF-encoding genes: *OsG1L2*, *OsFC1*, *OsMADS34* and *OsHOX14*. Interestingly, *OsMADS34* has been shown to be necessary for correct inflorescence development, further emphasizing the functional importance of this regulatory module (Kobayashi et al., 2012). *OsHOX14* can form heterodimers with *OsHOX12*, a gene that regulates panicle exertion (Gao et al., 2016). Overall, our network analysis allowed the identification of many interesting candidates, some of which have already been described in the context of panicle development and might be targets of OsG1L2 and other major players in this context. This analysis also provided suggestions for genes that might be involved in the same developmental pathway, regulating a similar set of genes.

Validation of GRNs by RT-qPCR

RT-qPCR experiments were carried out to validate some of the deregulated genes from subcluster C of the predicted GRN (Figure 5). We focused on genes that were already

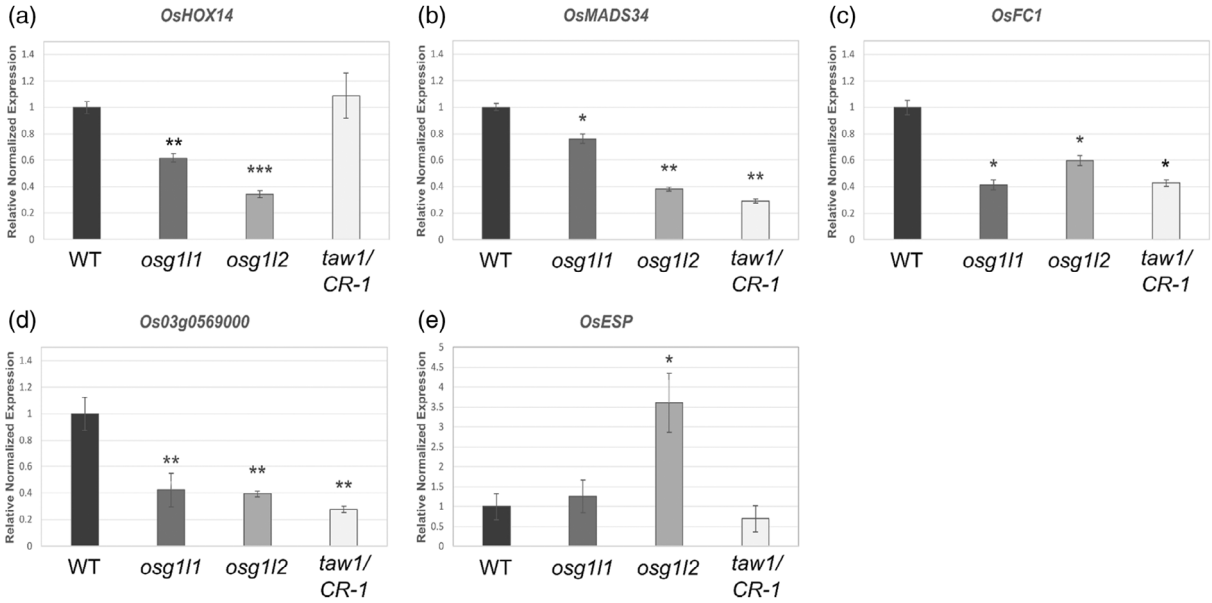

Figure 5. Expression analysis of subcluster C genes in the *osg1l1*, *osg1l2* and *taw1 CR-1* mutants.
Expression analysis of *OsHOX14* (a), *OsMADS34* (b), *OsFC1* (c), *Os03g0569000* (d) and *OsESP* (e) by quantitative real-time PCR in wild type (WT), *osg1l1*, *osg1l2* and *taw1 CR-1* mutants. The expression of *OsHOX14*, *OsMADS34*, *OsFC1* and *Os03g0569000* was normalized to that of *Elongation Factor 1* and the expression level of the wild type was set to 1. Student's *t*-test: ***$P < 0.001$; **$P < 0.01$; *$P < 0.05$.

proposed to be involved in inflorescence development, such as *OsHOX14*, *OsMADS34*, *OsFC1* and *OsESP* (Gao et al., 2010; Luan et al., 2019; Shao et al., 2018; Takeda et al., 2003). *Os03g0569000* was also analyzed as the GRN predicted it to be downstream of both *OsMADS34* and *OsG1L2*.

To include the *taw1 CR-1* mutant in this analysis, we generated a CRISPR-Cas9 mutant for this gene. The sgRNA was designed to target a region 275 bp downstream from the ATG start site (Figure S7). Two independent transformants had a homozygous insertion of 1 bp (Figure S7) at 293 bp from the translation start site. This mutation created a frameshift resulting in the formation of an aberrant protein, characterized by the disruption of the ALOG domain and of the putative NLS. For these reasons, the aberrant protein obtained is most likely not functional. The *taw1 CR-1* mutants closely resembled the phenotype of the already published missense mutant *taw1–3* (Yoshida et al., 2013).

The RT-qPCR was performed using three biological replicates of developing inflorescences enriched in PBMs and ePBMs/AMs of wild-type, *osg1l1*, *osg1l2* and *taw1 CR-1* plants.

As shown in Figure 5(a–e), RT-qPCR confirmed the downregulation of *OsHOX14*, *OsMADS34*, *OsFC1* and *Os03g0569000*, whereas *OsESP* was upregulated in the *osg1l2* mutant.

Expression analysis of the selected genes in the *osg1l1* mutant showed that *OsHOX14*, *OsMADS34*, *OsFC1* and *Os03g0569000* were also downregulated in this mutant background (Figure 5b–d), whereas the expression level of *OsESP* did not significantly differ from that of wild-type inflorescences (Figure 5e). Regarding the expression analysis performed in the *taw1 CR-1* mutant, *OsMADS34*, *OsFC1* and *Os03g0569000* were all downregulated in developing panicles, whereas the expression of neither *OsESP* nor *OsHOX14* was significantly changed with respect to that in the wild type. Overall, these results suggest that the genes analyzed within the *OsG1L2*-containing subcluster C (Figure 4) could have a genetic interaction, as predicted by the GRN. These analyses suggest that the *ALOG* genes under investigation participate in partially overlapping pathways governing panicle architecture in rice.

Loss of *OsHOX14* function causes changes in panicle architecture

The GRN subcluster C that contains *OsG1L2* has *OsMADS34*, *OsFC1* and *OsHOX14* as major components. *OsMADS34* and *OsFC1* have been studied intensively for their role in inflorescence development (Gao et al., 2010; Takeda et al., 2003), whereas for *OsHOX14* only an overexpression study has been reported (Shao et al., 2018). Therefore, we selected *OsHOX14* for further functional studies to validate the GRN-predicted involvement of this gene in inflorescence architecture. Notably, the RT-qPCR experiments, discussed above, suggest that *OsHOX14* is regulated by *OsG1L1* and *OsG1L2*, whereas *TAW1* does not seem to be involved.

OsHOX14 is a member of the homeodomain-leucine zipper (HD-Zip) TF family, and it is the rice ortholog of *HvHox2* in *Hordeum vulgare* (barley) that, together with its

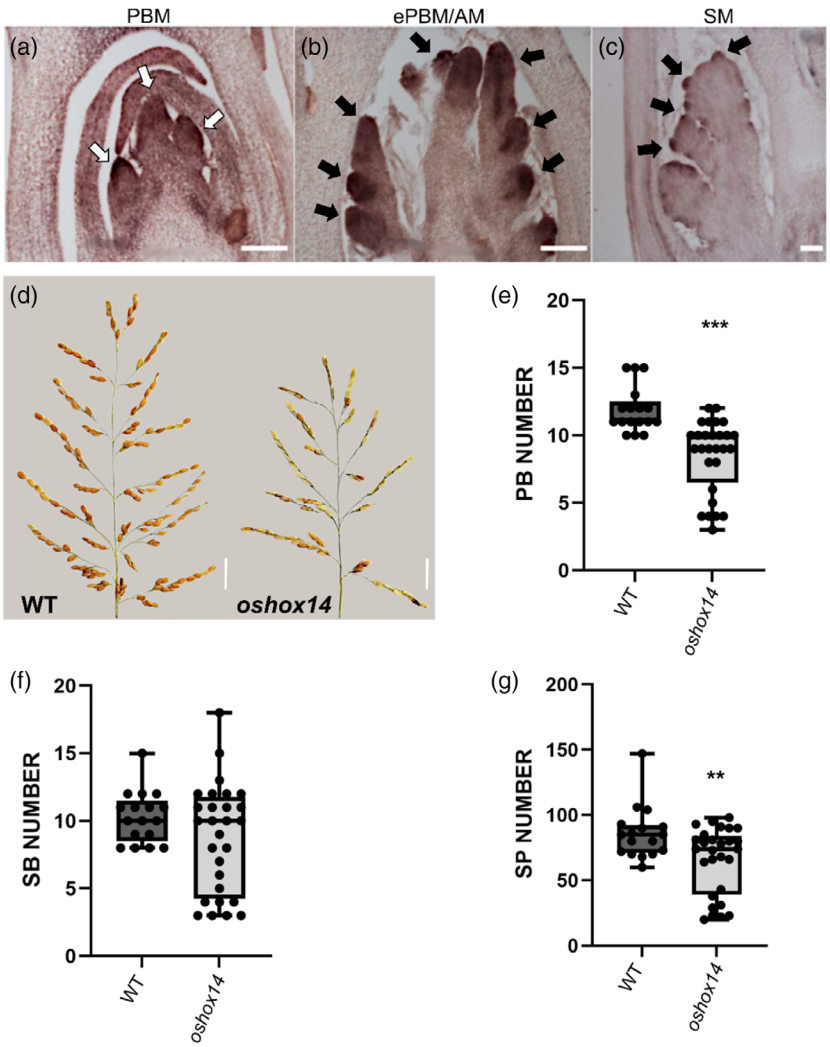

Figure 6. Expression and functional characterization of *OsHOX14*. *In situ* analysis of three developmental stages.
(a) Primary branch meristems PBMs; (b) elongated PBMs with axillary meristems (ePBMs/AMs); and (c) spikelet meristems (SMs). Scale bars: (a, b) 100 μm; (c) 50 μm. White (a) and black (b, c) arrows indicate the signal in the corresponding meristem type.
(d–g) Phenotypical analysis of panicle architecture in the wild type and the *oshox14* mutant. (d) Main panicles of wild type (WT) and *oshox14* (scale bars: 2 cm). Comparisons of (e) primary branch (PB) number, (f) secondary branch (SB) number and (g) spikelet (SP) number in WT and *oshox14* backgrounds. Student's *t*-test: ***$P < 0.001$; **$P < 0.01$.

recently diverged paralog *HvVrs1*, is responsible for the spike architecture of barley (Sakuma et al., 2010). Indeed, *OsHOX14*, like *OsG1L1* and *OsG1L2* was shown to be expressed in the reproductive meristem tissues (PBM, ePBM/AM and SM) (Harrop et al., 2016). The spatiotemporal expression of *OsHOX14* throughout early panicle development was assessed by RNA *in situ* hybridization analysis. *OsHOX14* was expressed in PBM, ePBM/AM and SM/FM, suggesting a putative role of this gene during reproductive meristem establishment (Figure 6a–c).

We generated a knockout mutant line for *OsHOX14* using the CRISPR-Cas9 genome editing system (Miao et al., 2013). A specific sgRNA was designed to target the first exon of the *OsHOX14* gene (Figure S8). T_0 transgenic plants were selected and genotyped. In the T_1 generation, three different mutant lines were obtained, one with a homozygous G deletion, one with a homozygous C insertion and one with a bi-allelic CG deletion and T insertion, at 7, 11, and 6 bp downstream of the start site, respectively. In all three cases, the different mutations led to a frameshift in the coding sequence and the formation of a premature stop codon, which resulted in the formation of a protein consisting of 22, 27 and 22 amino acids, respectively (Figure S8).

To evaluate the inflorescence phenotype of *oshox14*, a comparative analysis was performed on panicles belonging to five wild-type and five T_1 *oshox14* mutant plants (one plant carrying the homozygous C insertion mutation,

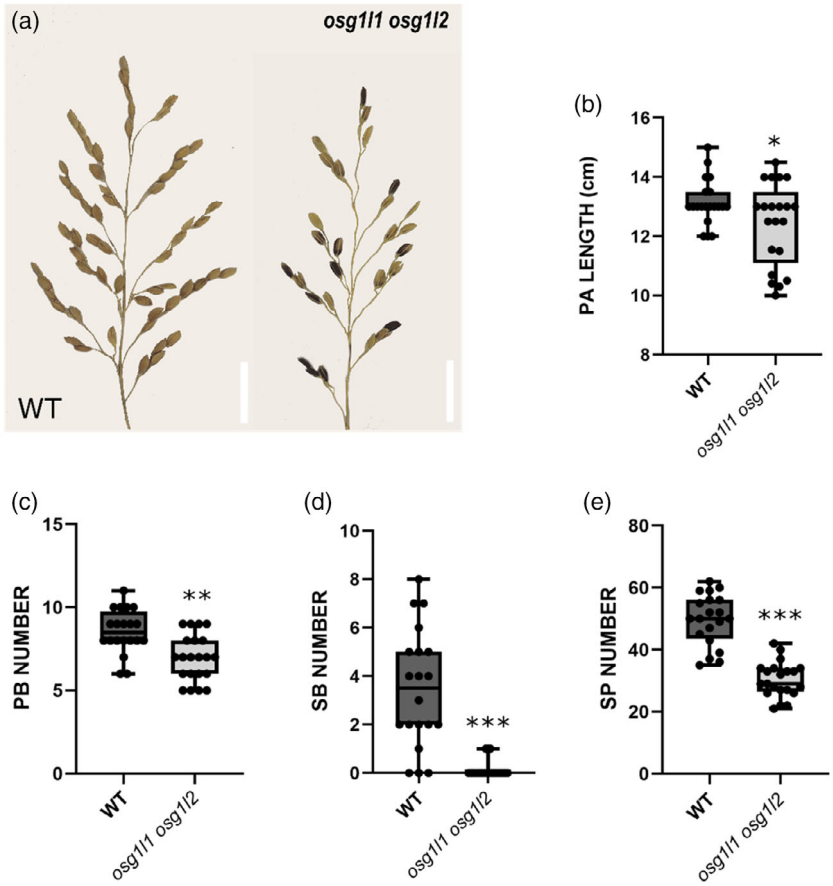

Figure 7. Phenotypical analysis of panicle architecture in wild type (WT) and the *osg1l1 osg1l2* double mutant.
(a) Main panicles of WT and the *osg1l1 osg1l2 double mutant* (scale bars: 2 cm). Comparisons of (b) panicle (PA) length, (c) primary branch (PB) number, (d) secondary branch (SB) number and (e) spikelet (SP) number in WT and *osg1l1 osg1l2* backgrounds. Student's *t*-test: ***$P < 0.001$; **$P < 0.01$; *$P < 0.05$.

one plant carrying the CG deletion and T insertion mutation, and three plants carrying the G deletion mutation). This analysis revealed that the *oshox14* mutants developed panicles with fewer PBs and spikelets than the wild-type plants. The number of SBs did not significantly differ from that of the wild type. In particular, the *oshox14* mutant plants produced panicles that developed on average three PBs and 20 spikelets fewer than the wild type (Figure 6d–g). Overall, this analysis showed that *OsHOX14* plays a role in inflorescence branching, as predicted by the GRN.

Osg1l1 osg1l2 double mutant phenotype

To investigate the genetic relationship between *OsG1L1* and *OsG1L2*, we generated the double mutant by crossing the *osg1l1* and *osg1l2* single mutants.

Homozygous double mutant grains exhibited difficulties in germination. During the vegetative phase, the overall structure of the plant did not present any obvious defects. However, the propagation of new generations of plants was difficult because of the very high rate of sterility in the *osg1l1 osg1l2* double mutant. We phenotypically compared the architecture of panicles of six wild-type and seven *osg1l1 osg1l2* double mutant plants. This comparative phenotypic analysis revealed that the *osg1l1 osg1l2* plants developed panicles that are shorter, with fewer PBs, extremely reduced SBs and fewer spikelets than the wild-type plants. In particular, the *osg1l1 osg1l2* double mutant plants produced panicles that were on average 1.5 cm shorter than the wild type and developed on average two PBs and 20 spikelets fewer than wild-type plants (Figure 7b,c,e). Interestingly, concerning the SBs, except the three panicles that developed only one SB each, none of the other panicles of the double mutant produced SBs (Figure 7d). This analysis indicates that combining the *osg1l1* and *osg1l2* mutants results in an enhancement of the reduction in SB formation, almost completely abolishing the development of these branches.

Furthermore, combining the single mutants caused a high rate of sterility, as only 6.2% of the spikelets produce viable grains, suggesting that *OsG1L1* and *OsG1L2* are redundantly involved in plant fertility. Indeed, the panicles analyzed each developed, on average, only two fertile grains.

DISCUSSION

Inflorescence architecture is a key agronomic trait that influences grain yield, and its development is finely regulated by genes involved in the specification of meristem identity and in the control of the transition from indeterminate to determinate growth. Therefore, identifying genes involved in inflorescence development promises to contribute to improved crop yield through breeding and biotechnological approaches.

In this study, we functionally characterized *OsG1L1* and *OsG1L2*, two rice genes belonging to the *ALOG* gene family. These two genes are likely to play an important role in the regulation of inflorescence architecture specification, acting as positive regulators of primary branch (PB) and secondary branch (SB) development. The role of *OsG1L1* and *OsG1L2* in such processes is suggested by their expression in the reproductive meristems, in a pattern similar to *TAW1*, an *ALOG* family member already known to be involved in the development of the rice inflorescence, by promoting indeterminate meristem identity (Yoshida et al., 2013). We compared the protein and promoter sequence of *OsG1L1*, *OsG1L2* and *TAW1* with those of *OsG1* and *OsTH1*, other *ALOG* genes already characterized in rice (Sato et al., 2014; Yoshida et al., 2009). Interestingly, neither *OsG1* nor *OsTH1* shows any meristematic expression. The protein sequence encoded by the five *ALOG* genes is quite conserved, showing an identity spanning from 54% to 79% (Figure S9). Of course, if identity calculation is restricted to the ALOG domains, then the percentage will be even higher, as shown in Figure S9, which has already been described by Naramoto et al. (2020).

Notably, an analysis of the promoter sequence revealed a subset of TFs that are predicted to bind motifs in *OsG1L1*, *OsG1L2* and *TAW1*, but not *OsG1* and *OsTH1* promoters, like members of the *AP2*, *NAM* and *MADS*-domain TF families (Table S5). This observation suggests that this subset of TFs might be important for the peculiar meristematic expression pattern of *OsG1L1*, *OsG1L2* and *TAW1*.

Phenotypical analysis of the *osg1l1* and *osg1l2* mutant inflorescences showed that the two single mutants developed shorter panicles with fewer spikelets and smaller grains, when compared with the wild type. Overall, the inflorescence architecture of *osg1l1* and *osg1l2* single mutants resembled the *taw1* mutant phenotype. Furthermore, SEM analysis revealed that the *osg1l1* and *osg1l2* mutants faced a premature switch from indeterminate ePBMs/AMs to determinate SMs. This observation was confirmed with *in situ* hybridization using the *FZP* spikelet identity meristem marker. The expression of *FZP* evidenced that spikelet identity determination happened earlier in the *osg1l1* and *osg1l2* mutants, suggesting that, like *TAW1*, both *OsG1L1* and *OsG1L2* repress the transition from indeterminate to determinate phase changes in the IMs (Figure 8). Based on these observations it is tempting to speculate that both *OsG1L1* and *OsG1L2* might regulate the overall architecture of the panicles with regards to the length of the rice inflorescence, and consequently the number of PBs that can develop, controlling the timing of IM abortion.

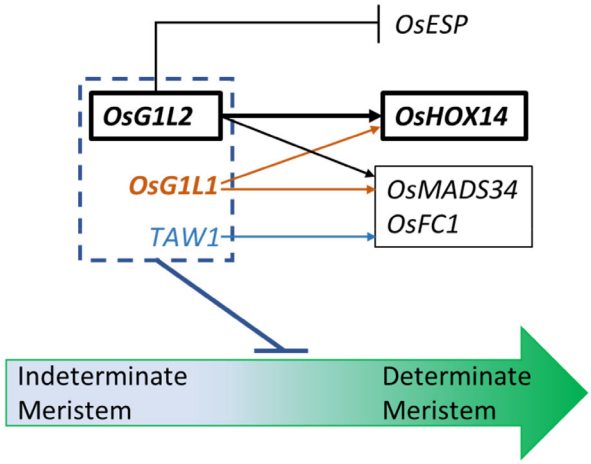

Figure 8. The regulatory network of the analysed *ALOG* genes. The gene regulatory network (GRN) of *OsG1L1*, *OsG1L2* and *TAW1* (dashed box) modulates the phase transition from indeterminate (light blue) to determinate (green) meristems. *ALOG*s regulate both unique (*OsESP*) or shared downstream genes (*OsMADS34 and OsFC1*). *OsHOX14* is a specific putative target of both *OsG1L1* and *OsG1L2*. (⊣ indicates negative regulation; ⟞ indicates positive regulation, the genes in bold are functionally characterized in this work).

The *osg1l1 osg1l2* double mutant showed an almost complete loss of SB formation, suggesting that the two genes act redundantly on the formation of these branches (Figure 2e).

The fact that the double mutant plants were almost completely sterile suggests that *OsG1L1* and *OsG1L2* also play an important role in the fertility of the plant. Indeed, in both RNA-seq and RT-qPCR analyses (Figure 1a,b), the expression of *OsG1L1* and OsG1L2 during FM formation and grain development overlapped, whereas *TAW1* was barely expressed in these tissues. It is further interesting to note that the expression of *OsG1L1* and *OsG1L2* also overlapped in mature grain tissues, and again that *TAW1* was more weakly expressed. These different patterns might explain the low germination rate of the *osg1l1 osg1l2* double mutant. Further analysis on fertility and grain development will need to be performed to understand the cause of these observations.

Expression analysis of the putative downstream genes of *TAW1* (Yoshida et al., 2013), *OsMADS22*, *OsMADS47* and *OsMADS55* in the *osg1l1* and *osg1l2* mutant backgrounds did not evidence any difference when compared with the wild type (Figure S5). The list of DEGs obtained

from our RNA-seq analysis of the *osg1l2* mutant inflorescences accords with these data, and also shows that other genes proposed to act downstream of TAW1, such as *OsMADS7*, *OsMADS8*, *OsMADS16*, *OsMADS3* and *OsMADS58*, all demonstrated a level of expression that was comparable with that in the wild type (Yoshida et al., 2013). These observations might suggest that, as being part of distinct phylogenetic groups, *OsG1L1* and *OsG1L2* may function in an inflorescence developmental pathway that acts in parallel with *TAW1*. However, as the downstream genes were identified by Yoshida et al. (2013) in the dominant *taw1-D* gain-of-function mutant it might well be possible that in our recessive single mutants we do not see significant changes in the expression of these downstream genes because of redundancy among *TAW1*, *OsG1L1* and/or *OsG1L2*. Future genetic experiments in which the different mutants will be combined in higher-order mutant combinations might clarify this.

The transcriptomic analysis of the *osg1l2* reproductive meristems revealed that some of the DEGs are indeed factors known to be involved in the determination of inflorescence architecture. For instance, in previous studies, the overexpression of *OsRCN1* and *OsRCN4* resulted in plants that produced panicles with an increased number of branches (Liu et al., 2013; Nakagawa et al., 2002), and the knockdown of all *RCN* genes resulted in shorter panicles with fewer SBs (Liu et al., 2013). This phenotype is similar to that observed in the *osg1l2* mutant, where *OsRCN1* and *OsRCN4* are both downregulated. Nakagawa et al. (2002) indicate a role for *RCN* genes in the suppression of SM identity that fits well with the evidence presented for the *OsG1L1* and *OsG1L2* genes as meristematic regulators. Furthermore, it is also interesting to note that recently it was reported that *OsRCN4* is regulated by OsMADS34 (Zhu et al., 2022). In the GRN that we propose, *PAP2/OsMADS34* falls in the same subcluster as *OsG1L2*. *OsMADS34* belongs to the *SEPALLATA* (*SEP*) subfamily of the MADS-box gene family and was previously reported as a positive regulator of SM development (Gao et al., 2010; Kobayashi et al., 2012). The phenotype of the *osmads34 osrcn4* double mutant is similar to the phenotypes observed in our *osg1l1* and *osg1l2* single mutants (Zhu et al., 2022). Together, all these observations suggest that *OsMADS34*, *OsRCN4*, *OsG1L1* and *OsG1L2*, and probably also *TAW1*, are involved in the same pathway controlling inflorescence architecture, but further analysis will be necessary to clarify the molecular genetic interactions between them.

Other examples to mention are *OsGATA6* and *OsGATA7*, two TFs that were downregulated in the *osg1l2* mutant. Knockdown and knockout mutants of *OsGATA6* and *OsGATA7* showed alterations in the architecture of the inflorescence: in particular, they developed panicles bearing fewer PBs and SBs (Zhang et al., 2018; Zhang et al., 2022). It is also interesting to mention that *OsGATA6* and *OsGATA7* were proposed to work in the pathway of Brassinosteroid signaling and that *OsGATA7* controls cell proliferation. It will be worth analyzing further whether the elongation of the PBs and the modification in grain size that we observe in our *osg1l2* background results from a different cell proliferation rate. Moreover, as *OsGATA6* and *OsGATA7* are located in a different subcluster than *OsG1L2* in the predicted GRN (Figure 4), it could be hypothesized that these two genes regulate inflorescence architecture in a parallel pathway.

Some genes that were upregulated in the *osg1l2* background had an expression level equal to zero in the wild-type background. One of them is *OsESP*, which encodes for a long non-coding RNA (Luan et al., 2019). In the semi-dominant *Epi-sp* mutant, the 3′ region of the transcribed region was characterized by a loss of DNA methylation, resulting in a strong upregulation of the gene causing the development of a denser and shorter panicle. It might well be that the reduction in panicle length observed in the *osg1l2* background is linked to the observed upregulation of *ESP*. It would be interesting to investigate whether the loss of *OsG1L2* activity leads to changes in the 3′ methylation of the *ESP* gene. *ESP* was one of the predicted putative direct targets of OsG1L2 within the GRN and according to our RT-qPCR experiments, its deregulation seems to be specific only for the *osg1l2* mutant as no upregulation was observed in the *osg1l1* and *taw1 CR-1* mutants. The GRN also indicated that *ESP* (together with eight other genes, still unknown and only expressed in the developing inflorescences of the *osg1l2* mutant) is a target of both *OsG1L2* and *OsFC1*. It is known that *OsFC1* controls panicle architecture as the null mutant developed shorter panicles (Cui et al., 2020). It might well be that during the reproductive phase OsFC1 represses *ESP*, together with OsG1L2.

Among the genes that were selected for real-time PCR validation, *OsHOX14* showed a strong downregulation in the *osg1l2* mutant, and to some extent also in the *osg1l1* mutant, but was not deregulated in the *taw1 CR-1* mutant. This result suggests that these *ALOG* genes regulate rice panicle development through partially overlapping pathways, as described in our model (Figure 8).

Notably, *OsHOX14* is a member of the HD-Zip TF family, members of which are known to play important roles in various aspects of plant development, morphogenesis, and responses to biotic and abiotic stresses in different species (Perotti et al., 2017; Sessa et al., 2018). The specific expression profile obtained through *in situ* hybridization confirmed the expression of *OsHOX14* in reproductive meristems, as reported by Harrop et al. (2016) and Shao et al. (2018). Furthermore, it is worth mentioning that the online RiceXPro tool (https://ricexpro.dna.affrc.go.jp) showed the expression of *OsHOX14* mainly in developing panicles and pistils, suggesting a specific role of this TF

during reproductive development. The CRISPR *oshox14* mutants that we generated confirmed a role for this gene in inflorescence development, as panicle architecture was impaired in these mutants. The *OsHOX14* overexpression lines generated by Shao et al. (2018) displayed dramatic phenotypes, such as a severe delay in growth at the seedling stage and difficulties with panicle exertion through stems and leaves. A mild overexpression line was analyzed for panicle development, which showed both a reduction in panicle length and PB number. As the ectopic expression of *OsHOX14* during the vegetative phase causes growth defects, it might well be that this caused pleiotropic effects on reproductive development. However, we cannot rule out the possibility that the knockout mutant caused a similar phenotype as the overexpression line because of the existence of regulatory loops and the dependence on threshold levels that could influence regulatory pathways (Prelich, 2012).

Taking all these observations together, it is tempting to hypothesize that *OsG1L1*, *OsG1L2* and *TAW1* act in partially overlapping pathways. Moreover, *OsG1L2* together with *OsG1L1* seems to act in pathways that include *OsHOX14*, *OsMADS34* and *OsFC1* (Figure 8). Finally, the functional analysis of *OsHOX14* indicated that the proposed GRN promises to be of value for the identification of new players in the first stages of inflorescence development.

EXPERIMENTAL PROCEDURES

Plant material and growth condition

For our experiments we used *O. sativa* ssp. *japonica*, cv. Nipponbare. The plants were grown for 8–10 weeks under long-day (LD) conditions (70% humidity, 16 h light at 28°C/8 h dark at 26°C) and then moved to short-day (SD) conditions (70% humidity, 12 h light at 28°C/12 h dark at 26°C) to induce flowering. *In vitro*, plants were germinated on MS-F medium (2,2 g L^{-1} MS + vitamins, 15 g L^{-1} sucrose, 1 L ddH_2O, with pH adjusted to 5.6 by adding KOH, 2.5 g L^{-1} gelrite) and were transplanted to soil after 15 days. Plants used for phenotypic analysis were grown in a transgenic glasshouse (located at the IRD center, Montpellier, France) in spring 2019 (grains have been sown in February 2019 and panicles collected in June) under natural day conditions at 28–30°C with humidity of 60%. Plants used for the RNA-seq experiment were grown in the C chamber at the NC State University Phytotron.

RNA isolation and cDNA synthesis

Total RNA from different tissues (roots, young and mature leaves, milk and mature grains) and from meristematic tissue enriched in IM, PBMs, ePBMs/AMs and SMs was extracted with the NucleoSpin® RNA Plant kit (MACHEREY-NAGEL, http://www.mn-net.com) and DNA contamination was removed using the TURBO DNA-free™ Kit in accordance with the manufacturer's instructions (ThermoFisher Scientific, https://www.thermofisher.com). The different tissues were sampled in liquid nitrogen using an optical microscope. The RNA was reverse transcribed using the ImProm-II™ Reverse Transcription System (Promega, https://www.promega.com) and the cDNA was used as a template in RT-qPCR reactions.

Transcriptome analysis

Eighty plants (40 wild-type plants and 40 *osg1l2* mutant plants) were sown in a growth chamber under LD conditions (70% humidity, 16 h light at 28°C/8 h dark at 26°C) at the NC State University Phytotron and, after 12 days of induction in SD conditions, were sampled. Fifty milligrams of tissue, corresponding to between eight and 10 meristems at early developmental stages, enriched in PBMs and ePBMs/AMs, was manually dissected using an optical microscope. RNA was extracted from the samples using the RNeasy Plant Mini Kit (Qiagen, https://www.qiagen.com). cDNA libraries were prepared using the NEBNext Ultra DNA Library Prep Kit for Illumina (E7370; New England Biolabs, https://international.neb.com), according to the manufacturer's instructions. The Novaseq6000 (Illumina, https://www.illumina.com) was used and sequencing was single-end stranded.

Data analysis

Raw RNA-seq data in fastq format for the wild type and the *osg1l2* mutant were processed and subsequently used for GRN inference with the TUXNET interface (https://github.com/rspurney/TuxNet; Spurney et al., 2019). For the processing of the raw RNA-seq data, the gff and fasta file of the reference genome (IRGSP-1.0) and gene name file was downloaded from The Rice Annotation Project Database (RAP-DB; https://rapdb.dna.affrc.go.jp/download/irgsp1.html) (Table S6). The gene IDs from rice TFs were downloaded from the plant transcription database (v4.0; http://planttfdb.gao-lab.org) and converted from MSU to RAP, with the manual addition of the *ALOG* gene family. Next, TUXNET uses EA-UTILS FASTQ-MCF (Aronesty, 2013) for pre-processing, HISAT2 (Kim et al., 2015) for genome alignment and CUFFLINKS (Trapnell et al., 2012) for differential expression analysis. The following xlsx files are generated by TUXNET: a file containing the FPKM values for each replicate (Table S3), a file with the DEGs identified with a *q*-value threshold of 0.05 and a $\log_2$(FC) of 1 (Table S4) and a file containing an average expression, a $\log_2$(FC) and a *q*-value (Table S7).

The principal component analysis (PCA) was performed in R with the RPKM file from TUXNET using the *prcomp* function from the STATS package and the PCA3D package (https://CRAN.R-project.org/package=pca3d) (Figure S10).

To infer the GRN in *osg1l2* and predict the causal relationships between target genes underlying the inflorescence phenotype in *osg1l2*, the differentially expressed TFs and genes identified in *osg1l2* with a *q*-value threshold of <0.05 and a $\log_2$(FC) > 1 or <−1 (Table S4) were selected. We manually added *OsG1L2* to the DEGs list, as the $\log_2$FC of *OsG1L2* was <1 (−0.885798). Within the TUXNET interface, RTP-STAR (Regression Tree Pipeline for Spatial, Temporal and Replicate data) leverages the replicate data of the wild type and *osg1l2* and consists of three parts: spatial clustering using the *k*-means method, network inference using GENIE 3 (regression tree with random forest approach) and edge sign (activation or repression) identification using the first-order Markov method. As options, we used 100 iterations when inferring the GRN and an edge proportion equal to 0.33. The table containing the final predicted network (Table S8) has been imported into CYTOSCAPE 3.8.0 (Shannon et al., 2003) to obtain a high-quality graphic representation of the predicted GRN. Different node shapes, colors, and sizes were used to represent TFs, down- or upregulation in *osg1l2*, and the number of interactions, respectively. The nodes within the network were clustered into different modules with the CYTOSCAPE plug-in CLUSTERMAKER 2 according to the available community clustering algorithm, an implementation of the Girvan–Newman fast greedy algorithm that uses connectivity to cluster nodes (Morris et al., 2011).

RT-qPCR analysis

Fresh meristematic tissue enriched in IMs, PBMs, ePBMs/AMs and SMs was collected in liquid nitrogen using an optical microscope. RNA was extracted with the NucleoSpin® RNA Set for NucleoZOL kit for high-purity products (MACHEREY-NAGEL).

The RT-qPCR analysis was carried out in a final volume of 12 μl in a Bio-Rad C1000™ thermal cycler (Bio-Rad, https://www.bio-rad.com), using 3 μl of a 1:10 dilution of cDNA, 0.2 μM (stock 10 mM) Forward and Reverse Primer, 6 μl of Sybr Green Super Mix 2X (Bio-Rad) and 2.6 μl of MQ H_2O.

The expression levels of *OsG1L1*(*LOC_Os02g07030*), *OsG1L2* (*LOC_Os06g46030*) and *TAW1* (*LOC_Os10g33780*) were evaluated using primer pairs RT2541/RT2542, RT1387/RT1389 and RT2543/RT2544, respectively. The RT-qPCR was performed with the following conditions: 95°C for 90 sec with 40 cycles of 95°C for 15 sec, 60°C for 10 sec and 60°C for 30 sec, and then 60°C for 10 sec.

The expression levels of *OsESP*(*Os01g0356951*), *OsMADS34/PAP2* (*LOC_Os03g54170*), *OsHOX14* (*LOC_Os07g39320*), *OsCEP6* (*LOC_Os08g37070.1*), *OsTB1/FC1* (*LOC_Os03g49880*) and *Os03g0569000* in the wild-type and *osg1l2* backgrounds were evaluated using primer pairs OSP2055/OSP2056, OSP0855/OSP0856, OSP1400/1401, OSP2043/OSP2044, OSP2045/OSP2046 and OSP 2059/OSP2060, under the following conditions: 95°C for 90sec, with 40 cycles of 95°C for 15 sec, 58°C for 10 sec and 60°C for 30 sec, and finally 60°C for 10 sec. Three biological replicates for each experiment were performed. Rice *Elongation Factor 1* (*EF1*) (*LOC_Os03g08010*) was used as an internal reference during the experiments. Primer sequences are listed in Table S9.

Tissue fixation and *in situ* hybridization

Rice reproductive meristems from the main stem at different stages of early panicle development were collected and fixed in FAA – ethanol 50% (Fluka, now Honeywell, https://lab.honeywell.com), acetic acid 5% (Sigma-Aldrich, https://www.sigmaaldrich.com) and formaldehyde 3.7% (Sigma-Aldrich) (v/v/v) – infiltrated under mild vacuum conditions for 15 min in ice. After 1 h 45 min, the samples were washed three times for 10 min in EtOH 70% and conserved at 4°C; they were dehydrated in a series of increasing graded ethanol, transferred to bioclear (Bioptica, https://www.bioptica.co.uk) and then embedded in Paraplast X-TRA® (Sigma-Aldrich). To generate the sense and antisense probes, gene fragments were amplified from cDNA using gene-specific primers (Table S9), cloned into pGEM®-T Easy Vector and confirmed by sequencing. Digoxigenin-labeled antisense and sense RNA probes were transcribed and labeled with pGEM®-T Easy with T7/SP6 RNA polymerase (Promega), according to the manufacturer's instructions and using the DIG RNA labelling mix (Roche, https://www.roche.com). Paraplast-embedded tissues were sliced on an RM2155 microtome (Leica, https://www.leica-microsystems.com) at a thickness of 8 μm and hybridized as described by Caselli et al. (2020), with minor modifications. Immunodetection was carried out with anti-digoxigenin-AP Fab fragment (Roche) and BCIP-NBT color development substrate (Promega), as specified by the manufacturer. Sample images were acquired with a Zeiss Axiophot D1 microscope with an Axiocam MRc 5 at different magnifications (Zeiss, https://www.zeiss.com).

With regards to *FZP*, the probes were designed as already described in Komatsu et al., 2003.

IM analysis by SEM

SEM samples were prepared as described by Mizzotti et al. (2015) by gold coating them using a sputter coater (SEMPrep2; NanoScience Instruments, https://www.nanoscience.com), followed by observation with an FESEM SIGMA Scanning Electron Microscope (Zeiss).

Generation of CRISPR-Cas9 constructs

For the generation of *osg1l1*, *osg1l2* and *oshox14* (LOC_Os07g39320) single knockout mutants, 20-bp specific protospacers (Table S9) for each gene were selected using the CRISPR-P database (http://cbi.hzau.edu.cn/crispr/) and cloned into the *BsaI* site of pOs-sgRNA entry vectors under the U3 promoter and then combined into the destination vector containing the Cas9 under *Zea mays* (maize) Ubiquitin Promoter using the Gateway® LR Clonase II Enzyme mix, following the procedure reported by Miao et al. (2013) and already followed by Lacchini et al. (2020).

Bacterial and plant transformation

For bacterial transformation, we used *Escherichia coli* electrocompetent cell (DH10b strains) and *Agrobacterium tumefaciens* electrocompetent cell (EH105 strain).

All final constructs were used to transform embryogenic calli obtained from *O. sativa* ssp. *japonica* cv. Nipponbare grains, according to the protocol described by Hiei et al. (1994) and Toki (1997).

Mutant screening in transgenic plants

Genomic DNA was extracted from T_0 hygromycin-resistant rice plants and genotyped by PCR using primers specific for the Cas9 construct Atp5706/Atp5718 (Table S9). Subsequently, from the positive plants, DNA fragments across the target sites were amplified through PCR using gene-specific primer pairs (Table S9). The PCR amplicons were purified and sequenced. The chromatograms obtained were analyzed and compared with wild-type sequences with FINCHTV searching for mutations.

Phenotypical analysis of panicles and grains

To perform phenotypical analysis, 15, 19 and 20 panicles from the main tiller were collected from wild-type, *osg1l1* and *osg1l2* plants, respectively. Each panicle was attached to A4 white paper and all panicle branches were spread and blocked with transparent sticks. Each paper with panicle and scale bar was put on an image capturing system consisting of portable camera stand and two RB 218N HF lighting units. The pictures were processed into P-TRAP software. The analysis was perfomed as described by A L-Tam et al. (2013). The results were statistically analyzed by one-way analysis of variance (ANOVA), followed by Tukey's test, and represented with PRISM 8 (GraphPad, https://www.graphpad.com).

To perform the phenotypical analysis on wild-type and *oshox14* plants, all the panicles produced by five wild-type and five *oshox14* plants were collected. For each panicle, the number of PBs, SBs and spikelets/grains (SPs) was manually calculated. The results were statistically analysed with a Student's *t*-test and graphically represented with PRISM 8.

At least 100 grains were analyzed for each genotype (*osg1l1*, *osg1l2* and WT). Images of the grains were acquired using a Leica MZ6 stereomicroscope in conjunction with a Leica DFC280 camera at different magnifications; each image was then processed with SMART GRAIN (Tanabata et al., 2012). The results obtained were statistically analyzed with a one-way ANOVA, followed by Tukey's test and represented with PRISM 8.

Promoter analysis and protein alignment

The promoter analysis was performed using the Plant Promoter Analysis Navigator (PlantPAN3; http://PlantPAN.itps.ncku.edu.tw). Specifically, gene group analysis was used to determine the TFs and their binding sites within the promoters of *OsG1*, *OsG1L1*, *OsG1L2*, *TAW1* and *OsTH1*. The default parameters were used, with the coordinates of the promoter here defined as 1000 bp upstream and 100 bp downstream of the transcription start site (Chow et al., 2019). The protein alignment was performed using UniProt (https://www.uniprot.org/align).

ACCESSION NUMBERS

Sequences from this article can be found in the GenBank/EMBL databases under the following accession numbers: *OsG1L1*, LOC_Os02g07030; *OsG1L2*, LOC_Os06g46030; *TAW1*, LOC_Os10g33780; *OsESP*, Os01g0356951; *OsMADS34/PAP2*, LOC_Os03g54170; *OsHOX14*, LOC_Os07g39320; *OsCEP6*, LOC_Os08g37070.1; *OsTB1/FC1*, LOC_Os03g49880; Os03g0569000; *OsEF1*, LOC_Os03g08010.

AUTHOR CONTRIBUTIONS

MMK and VG conceived and designed this research. EF, VMB, EC, IUD, GO-A, LVdB, RS and EL carried out and interpreted the experiments. HA and SJ contributed to experimental design and analysis. VMB, EF, VG and MMK wrote the article, with contributions from all authors.

ACKNOWLEDGEMENTS

We thank Andrea Guazzotti, Andrea Finocchio, Stefano Buratti, Cecilia Bertone and Marco Maffei for valuable discussions and technical support. Furthermore, we thank Mario Beretta and Valerio Parravicini for their help with taking care of the rice plants. Part of this work was carried out at NOLIMITS, an advanced imaging facility established by the Università degli Studi di Milano. This work was supported by MUR PRIN2017_2017N5LBZK. The PhD fellowships for EF and VMB were supported by the Doctorate School in Molecular and Cellular Biology, Università degli Studi di Milano. EF was supported by H2020-MSCA-RISE-2015 ExpoSEED (proposal number 691109). Open Access Funding provided by Universita degli Studi di Milano within the CRUI-CARE Agreement.

CONFLICT OF INTEREST

The authors declare that they have no conflicts of interest associated with this work.

SUPPORTING INFORMATION

Additional Supporting Information may be found in the online version of this article.

Figure S1. Gene structure and wild-type and mutant protein alignment of *OsG1L1*.

Figure S2. Gene structure and wild-type and mutant protein alignment of *OsG1L2*.

Figure S3. Chromatogram showing the type of mutation and phenotypical analysis of *osg1l2* mutant (C insertion).

Figure S4. Size measurements of wild-type, *osg1l1* and *osg1l2* grains.

Figure S5. Expression analysis of *OsMADS22*, *OsMADS47* and *OsMADS55* in wild-type, *osg1l1* and *osg1l2* backgrounds.

Figure S6. Expression pattern of *FZP* analyzed by *in situ* hybridization in wild type, *osg1l1* and *osg1l2*.

Figure S7. Gene structure and wild-type and mutant protein alignment of *TAW1*.

Figure S8. Gene structure and wild-type and mutant protein alignment of *OsHOX14*.

Figure S9. Protein alignment for OsG1 (Os07g0139300), OsG1L1 (Os02g0166800), OsG1L2 (Os06g0672400), OsTH1 (Os02g0811000) and TAW1 (Os10g0478000).

Figure S10. PCA output.

Table S1. Phenotypical traits analyzed in wild-type, *osg1l1* and *osg1l2* plants.

Table S2. Area, length and width of wild-type, *osg1l1* and *osg1l2* grains.

Table S3. FPKM values for each replica.

Table S4. Genes differentially expressed between the wild-type plants and the *osg1l2* mutants.

Table S5. List of transcription factors that are predicted to bind motifs in *OsG1L1*, *OsG1L2* and *TAW1* promoters.

Table S6. List of gene names.

Table S7. Average gene expression, $\log_2$(fold change) and *q*-value in the wild type and the *osg1l2* mutant.

Table S8. Final predicted GRN.

Table S9. Primers used in this article.

REFERENCES

A L-Tam, F., Adam, H., Anjos, A.D., Lorieux, M., Larmande, P., Ghesquière, A. *et al.* (2013) P-TRAP: a panicle TRAit phenotyping tool. *BMC Plant Biology*, **13**, 122. Available from: https://doi.org/10.1186/1471-2229-13-122

Aronesty, E. (2013) Comparison of sequencing utility programs. *The Open Bioinformatics Journal*, **7**(1), 1–8. Available from: https://doi.org/10.2174/1875036201307010001

Bai, X., Huang, Y., Mao, D., Wen, M., Zhang, L. & Xing, Y. (2016) Regulatory role of FZP in the determination of panicle branching and spikelet formation in rice. *Scientific Reports*, **6**, 1–11. Available from: https://doi.org/10.1038/srep19022

Bommert, P., Satoh-Nagasawa, N., Jackson, D. & Hirano, H.Y. (2005) Genetic and evolution of grass inflorescence and flower development in grasses. *Plant and Cell Physiology*, **46**, 69–78. Available from: https://doi.org/10.1093/pcp/pci504

Caselli, F., Zanarello, F., Kater, M.M., Battaglia, R. & Gregis, V. (2020) Crop reproductive meristems in the genomic era: a brief overview. *Biochemical Society Transactions*, **48**(3), 853–865. Available from: https://doi.org/10.1042/BST20190441

Cheng, X., Jiang, H., Zhang, J., Qian, Y., Zhu, S. & Cheng, B. (2010) Overexpression of type-A rice response regulators, OsRR3 and OsRR5, results in lower sensitivity to cytokinins. *Genetics and Molecular Research: GMR*, **9**(1), 348–359. Available from: https://doi.org/10.4238/vol9-1gmr739

Chow, C.N., Lee, T.Y., Hung, Y.C., Li, G.Z., Tseng, K.C., Liu, Y.H. *et al.* (2019) Plantpan3.0: a new and updated resource for reconstructing transcriptional regulatory networks from chip-seq experiments in plants. *Nucleic Acids Research*, **47**(D1), D1155–D1163. Available from: https://doi.org/10.1093/nar/gky1081

Cui, Y., Hu, X., Liang, G., Feng, A., Wang, F., Ruan, S. *et al.* (2020) Production of novel beneficial alleles of a rice yield-related QTL by CRISPR/Cas9. *Plant Biotechnology Journal*, **18**(10), 1987–1989. Available from: https://doi.org/10.1111/pbi.13370

Fujishiro, Y., Agata, A., Ota, S., Ishihara, R., Takeda, Y., Kunishima, T. *et al.* (2018) Comprehensive panicle phenotyping reveals that qSrn7/FZP influences higher-order branching. *Scientific Reports*, **8**(1), 1–9. Available from: https://doi.org/10.1038/s41598-018-30395-9

Gao, S., Fang, J., Xu, F., Wang, W. & Chu, C. (2016) Rice HOX12 regulates panicle exsertion by directly modulating the expression of ELONGATED UPPERMOST INTERNODE1. *Plant Cell*, **28**(3), 680–695. Available from: https://doi.org/10.1105/tpc.15.01021

Gao, X., **Liang, W.**, **Yin, C.**, **Ji, S.**, **Wang, H.**, **Su, X.** ***et al.*** (2010) The SEPALLATA-like gene OsMADS34 is required for rice inflorescence and spikelet development. *Plant Physiology*, **153**(2), 728–740. Available from: https://doi.org/10.1104/pp.110.156711

Hakata, M., **Kuroda, M.**, **Ohsumi, A.**, **Hirose, T.**, **Nakamura, H.**, **Muramatsu, M.** ***et al.*** (2012) Overexpression of a rice tify gene increases grain size through enhanced accumulation of carbohydrates in the stem. *Bioscience, Biotechnology and Biochemistry*, **76**(11), 2129–2134. Available from: https://doi.org/10.1271/bbb.120545

Hake, S. (2008) Inflorescence architecture: the transition from branches to flowers. *Current Biology*, **18**(23), R1106–R1108. Available from: https://doi.org/10.1016/j.cub.2008.10.024

Han, Y., **Yang, H.** & **Jiao, Y.** (2014) Regulation of inflorescence architecture by cytokinins. *Frontiers in Plant Science*, **5**, 669. Available from: https://doi.org/10.3389/fpls.2014.00669

Harrop, T.W.R., **Ud Din, I.**, **Gregis, V.**, **Osnato, M.**, **Jouannic, S.**, **Adam, H.** ***et al.*** (2016) Gene expression profiling of reproductive meristem types in early rice inflorescences by laser microdissection. *Plant Journal*, **86**(1), 75–88. Available from: https://doi.org/10.1111/tpj.13147

Hiei, Y., **Ohta, S.**, **Komari, T.** & **Kumashiro, T.** (1994) Efficient transformation of rice (*Oryza sativa* L.) mediated by *Agrobacterium* and sequence analysis of the boundaries of the T-DNA. *The Plant Journal*, **6**(2), 271–282. Available from: https://doi.org/10.1046/j.1365-313X.1994.6020271.x

Huang, L., **Hua, K.**, **Xu, R.**, **Zeng, D.**, **Wang, R.**, **Dong, G.** ***et al.*** (2021) The LARGE2-APO1/APO2 regulatory module controls panicle size and grain number in rice. *The Plant Cell*, **33**, 1212–1228. Available from: https://doi.org/10.1093/plcell/koab041

Hudson, D., **Guevara, D.**, **Hand, A.**, **Xu, Z.**, **Hao, L.**, **Chen, X.** ***et al.*** (2013) Rice cytokinin GATA transcription factor1 regulates chloroplast development and plant architecture. *Plant Physiology*, **162**, 132–144. Available from: https://doi.org/10.1104/pp.113.217265

Ikeda-Kawakatsu, K., **Maekawa, M.**, **Izawa, T.**, **Itoh, J.I.** & **Nagato, Y.** (2012) ABERRANT PANICLE ORGANIZATION 2/RFL, the rice ortholog of Arabidopsis LEAFY, suppresses the transition from inflorescence meristem to floral meristem through interaction with APO1. *Plant Journal*, **69**(1), 168–180. Available from: https://doi.org/10.1111/j.1365-313X.2011.04781.x

Ikeda-Kawakatsu, K., **Yasuno, N.**, **Oikawa, T.**, **Iida, S.**, **Nagato, Y.**, **Maekawa, M.** ***et al.*** (2009) Expression level of ABERRANT PANICLE ORGANIZATION1 determines rice inflorescence form through control of cell proliferation in the meristem. *Plant Physiology*, **150**(2), 736–747. Available from: https://doi.org/10.1104/pp.109.136739

Iyer, L.M. & **Aravind, L.** (2012) ALOG domains: provenance of plant homeotic and developmental regulators from the DNA-binding domain of a novel class of DIRS1-type retroposons. *Biology Direct*, **7**(1), 1. Available from: https://doi.org/10.1186/1745-6150-7-39

Jain, M., **Kaur, N.**, **Garg, R.**, **Thakur, J.K.**, **Tyagi, A.K.** & **Khurana, J.P.** (2006) Structure and expression analysis of early auxin-responsive aux/IAA gene family in rice (*Oryza sativa*). *Functional and Integrative Genomics*, **6**(1), 47–59. Available from: https://doi.org/10.1007/s10142-005-0005-0

Kim, D., **Langmead, B.** & **Salzberg, S.L.** (2015) HISAT: a fast spliced aligner with low memory requirements. *Nature Methods*, **12**(4), 357–360. Available from: https://doi.org/10.1038/nmeth.3317

Kobayashi, K., **Yasuno, N.**, **Sato, Y.**, **Yoda, M.**, **Yamazaki, R.**, **Kimizu, M.** ***et al.*** (2012) Inflorescence meristem identity in rice is specified by overlapping functions of three AP1/FUL-like MADS box genes and PAP2, a SEPALLATA MADS box gene. *Plant Cell*, **24**(5), 1848–1859. Available from: https://doi.org/10.1105/tpc.112.097105

Komatsu, M., **Chujo, A.**, **Nagato, Y.**, **Shimamoto, K.** & **Kyozuka, J.** (2003) Frizzy panicle is required to prevent the formation of axillary meristems and to establish floral meristem identity in rice spikelets. *Development*, **130**(16), 3841–3850. Available from: https://doi.org/10.1242/dev.00564

Lacchini, E., **Kiegle, E.**, **Castellani, M.**, **Adam, H.**, **Jouannic, S.**, **Gregis, V.** ***et al.*** (2020) CRISPR-mediated accelerated domestication of African rice landraces. *PLoS One*, **15**(3), 1–12. Available from: https://doi.org/10.1371/journal.pone.0229782

Li, N., **Wang, Y.**, **Lu, J.** & **Liu, C.** (2019) Genome-wide identification and characterization of the ALOG domain genes in rice. *International Journal of Genomics*, **2019**, 1–13. Available from: https://doi.org/10.1155/2019/2146391

Liu, C., **Teo, Z.W.N.**, **Bi, Y.**, **Song, S.**, **Xi, W.**, **Yang, X.** ***et al.*** (2013) A conserved genetic pathway determines inflorescence architecture in Arabidopsis and rice. *Developmental Cell*, **24**(6), 612–622. Available from: https://doi.org/10.1016/j.devcel.2013.02.013

Luan, X., **Liu, S.**, **Ke, S.**, **Dai, H.**, **Xie, X.M.**, **Hsieh, T.F.** ***et al.*** (2019) Epigenetic modification of ESP, encoding a putative long noncoding RNA, affects panicle architecture in rice. *Rice*, **12**(1), 20. Available from: https://doi.org/10.1186/s12284-019-0282-1

Miao, J., **Guo, D.**, **Zhang, J.**, **Huang, Q.**, **Qin, G.**, **Zhang, X.** ***et al.*** (2013) Targeted mutagenesis in rice using CRISPR-Cas system. *Cell Research*, **23**(10), 1233–1236. Available from: https://doi.org/10.1038/cr.2013.123

Mizzotti, C., **Fambrini, M.**, **Caporali, E.**, **Masiero, S.** & **Pugliesi, C.** (2015) A CYCLOIDEA-like gene mutation in sunflower determines an unusual floret type able to produce filled achenes at the periphery of the pseudanthium. *Botany*, **93**(3), 171–181. Available from: https://doi.org/10.1139/cjb-2014-0210

Morris, J.H., **Apeltsin, L.**, **Newman, A.M.**, **Baumbach, J.**, **Wittkop, T.**, **Su, G.** ***et al.*** (2011) ClusterMaker: a multi-algorithm clustering plugin for Cytoscape. *BMC Bioinformatics*, **12**, 1–14. Available from: https://doi.org/10.1186/1471-2105-12-436

Nakagawa, M., **Shimamoto, K.** & **Kyozuka, J.** (2002) Overexpression of RCN1 and RCN2, rice TERMINAL FLOWER 1 CENTRORADIALIS homologs, confers delay of phase transition and altered panicle morphology in rice. *Plant Journal*, **29**, 743–750.

Naramoto, S., **Hata, Y.** & **Kyozuka, J.** (2020) The origin and evolution of the ALOG proteins, members of a plant-specific transcription factor family, in land plants. *Journal of Plant Research*, **133**(3), 323–329. Available from: https://doi.org/10.1007/s10265-020-01171-6

Ooka, H., **Satoh, K.**, **Doi, K.**, **Nagata, T.**, **Otomo, Y.**, **Murakami, K.** ***et al.*** (2003) Comprehensive analysis of NAC family genes in *Oryza sativa* and *Arabidopsis thaliana*. *DNA Research*, **10**(6), 239–247.

Perotti, M.F., **Ribone, P.A.** & **Chan, R.L.** (2017) Plant transcription factors from the homeodomain-leucine zipper family I. role in development and stress responses. *IUBMB Life*, **69**(5), 280–289. Available from: https://doi.org/10.1002/iub.1619

Prelich, G. (2012) Gene overexpression: uses, mechanisms, and interpretation. *Genetics*, **190**(3), 841–854. Available from: https://doi.org/10.1534/genetics.111.136911

Ruelens, P., **De Maagd, R.A.**, **Proost, S.**, **Theißen, G.**, **Geuten, K.** & **Kaufmann, K.** (2013) FLOWERING LOCUS C in monocots and the tandem origin of angiosperm-specific MADS-box genes. *Nature Communications*, **4**, 2280. Available from: https://doi.org/10.1038/ncomms3280

Sakuma, S., **Pourkheirandish, M.**, **Matsumoto, T.**, **Koba, T.** & **Komatsuda, T.** (2010) Duplication of a well-conserved homeodomain-leucine zipper transcription factor gene in barley generates a copy with more specific functions. *Functional and Integrative Genomics*, **10**(1), 123–133. Available from: https://doi.org/10.1007/s10142-009-0134-y

Sato, D.S., **Ohmori, Y.**, **Nagashima, H.**, **Toriba, T.** & **Hirano, H.Y.** (2014) A role for TRIANGULAR HULL1 in fine-tuning spikelet morphogenesis in rice. *Genes and Genetic Systems*, **89**(2), 61–69. Available from: https://doi.org/10.1266/ggs.89.61

Sessa, G., **Carabelli, M.**, **Possenti, M.**, **Morelli, G.** & **Ruberti, I.** (2018) Multiple links between HD-zip proteins and hormone networks. *International Journal of Molecular Sciences*, **19**(12), 4047. Available from: https://doi.org/10.3390/ijms19124047

Shannon, P., **Markiel, A.**, **Ozier, O.**, **Baliga, N.**, **Wang, J.**, **Ramage, D.** ***et al.*** (2003) Cytoscape: a software environment for integrated models. *Genome Research*, **13**(22), 426. Available from: https://doi.org/10.1101/gr.1239303.metabolite

Shao, J., **Haider, I.**, **Xiong, L.**, **Zhu, X.**, **Hussain, R.M.F.**, **Övernäs, E.** ***et al.*** (2018) Functional analysis of the HD-zip transcription factor genes Oshox12 and Oshox14 in rice. *PLoS One*, **13**(7), e0199248. Available from: https://doi.org/10.1371/journal.pone.0199248

Shrestha, R., **Gómez-Ariza, J.**, **Brambilla, V.** & **Fornara, F.** (2014) Molecular control of seasonal flowering in rice, arabidopsis and temperate cereals. *Annals of Botany*, **114**(7), 1445–1458. Available from: https://doi.org/10.1093/aob/mcu032

Spurney, R.J., **Van den Broeck, L.**, **Clark, N.M.**, **Fisher, A.P.**, **de Luis Balaguer, M.A.** & **Sozzani, R.** (2019) Tuxnet: a simple interface to process RNA sequencing data and infer gene regulatory networks. *Plant Journal*, **101**, 716–730. Available from: https://doi.org/10.1111/tpj.14558

Takeda, T., **Suwa, Y.**, **Suzuki, M.**, **Kitano, H.**, **Ueguchi-Tanaka, M.**, **Ashikari, M.** ***et al.*** (2003) The OsTB1 gene negatively regulates lateral branching in

rice. *The Plant Journal: For Cell and Molecular Biology*, **33**(3), 513–520. Available from: https://doi.org/10.1046/j.1365-313x.2003.01648.x

Tanabata, T., **Shibaya, T.**, **Hori, K.**, **Ebana, K.** & **Yano, M.** (2012) SmartGrain: high-throughput phenotyping software for measuring seed shape through image analysis. *Plant Physiology*, **160**(4), 1871–1880. Available from: https://doi.org/10.1104/pp.112.205120

Tanaka, W., **Pautler, M.**, **Jackson, D.** & **Hirano, H.-Y.** (2013) Grass meristems II: inflorescence architecture, flower development and meristem fate. *Plant and Cell Physiology*, **54**(3), 313–324. Available from: https://doi.org/10.1093/pcp/pct016

Toki, S. (1997) Rapid and efficient agrobacterium-mediated transformation in rice. *Plant Molecular Biology Reporter*, **15**(1), 16–21. Available from: https://doi.org/10.1007/BF02772109

Trapnell, C., **Roberts, A.**, **Goff, L.**, **Pertea, G.**, **Kim, D.**, **Kelley, D.R.** ***et al.*** (2012) Differential gene and transcript expression analysis of RNA-seq experiments with TopHat and cufflinks. *Nature Protocols*, **7**(3), 562–578. Available from: https://doi.org/10.1038/nprot.2012.016

Van Ooijen, G., **Mayr, G.**, **Kasiem, M.M.A.**, **Albrecht, M.**, **Cornelissen, B.J.C.** & **Takken, F.L.W.** (2008) Structure-function analysis of the NB-ARC domain of plant disease resistance proteins. *Journal of Experimental Botany*, **59**(6), 1383–1397. Available from: https://doi.org/10.1093/jxb/ern045

Wang, J., **Zhang, Q.**, **Wang, Y.**, **Huang, J.**, **Luo, N.**, **Wei, S.** & **Jin, J.** (2019) Analysing the rice young panicle transcriptome reveals the gene regulatory network controlled by TRIANGULAR HULL1. *Rice*, **12**(1), 1–10. https://doi.org/10.1186/s12284-019-0265-2

Wu, K.L., **Guo, Z.J.**, **Wang, H.H.** & **Li, J.** (2005) The WRKY family of transcription factors in rice and Arabidopsis and their origins. *DNA Research*, **12**(1), 9–26. Available from: https://doi.org/10.1093/dnares/12.1.9

Yoshida, A., **Sasao, M.**, **Yasuno, N.**, **Takagi, K.**, **Daimon, Y.**, **Chen, R.** ***et al.*** (2013) TAWAWA1, a regulator of rice inflorescence architecture, functions through the suppression of meristem phase transition. *Proceedings of the National Academy of Sciences of the United States of America*, **110**(2), 767–772. Available from: https://doi.org/10.1073/pnas.1216151110

Yoshida, A., **Suzaki, T.**, **Tanaka, W.** & **Hirano, H.Y.** (2009) The homeotic gene long sterile lemma (G1) specifies sterile lemma identity in the rice spikelet. *Proceedings of the National Academy of Sciences of the United States of America*, **106**(47), 20103–20108. Available from: https://doi.org/10.1073/pnas.0907896106

Zhang, Y.J., **Zhang, Y.**, **Zhang, L.**, **He, J.**, **Xue, H.**, **Wang, J.** ***et al.*** (2022) *OsGATA6* regulates rice heading date and grain number per panicle. *Journal of Experimental Botany*, **erac247**, 6133–6149. Available from: https://doi.org/10.1093/jxb/erac247

Zhang, Y.J., **Zhang, Y.**, **Zhang, L.L.**, **Huang, H.Y.**, **Yang, B.J.**, **Luan, S.** ***et al.*** (2018) OsGATA7 modulates brassinosteroids-mediated growth regulation and influences architecture and grain shape. *Plant Biotechnology Journal*, **16**, 1261–1264. Available from: https://doi.org/10.1111/pbi.12887

Zhu, W., **Yang, L.**, **Wu, D.**, **Meng, Q.**, **Deng, X.**, **Huang, G.** ***et al.*** (2022) Rice SEPALLATA genes OsMADS5 and OsMADS34 cooperate to limit inflorescence branching by repressing the TERMINAL FLOWER1-like gene RCN4. *New Phytologist*, **233**(4), 1682–1700. Available from: https://doi.org/10.1111/nph.1785